Environmental Science: Atmospheres

ROYAL SOCIETY OF CHEMISTRY

PAPER

View Article Online
View Journal | View Issue

Cite this: *Environ. Sci.: Atmos.*, 2025, **5**, 1119

Characterising changes in the methane response of a semiconductor-based metal oxide sensor over time

Adil Shah, *[a] Olivier Laurent,[a] Grégoire Broquet,[a] Clément Romand[b] and Philippe Ciais[a]

The semiconductor-based Figaro Taguchi Gas Sensor (TGS) is sensitive to reducing gases, including methane. TGS methane response can be characterised by using the ratio between resistance in the presence of methane mole fraction ($[CH_4]$) enhancements and a reference resistance, representative of sampling under the same environmental conditions and with the same background gas composition, but at a reference $[CH_4]$ level. Effects of environmental variables, including water mole fraction ($[H_2O]$), are expected to cancel in this resistance ratio, allowing for independent $[CH_4]$ characterisation. This work seeks to examine the cause of changes in $[CH_4]$ resistance ratio characterisation over time, including the hypothesis that resistance ratios are independent of $[H_2O]$. Precise gas blends were sampled under controlled conditions during sensor characterisation in synthetic air (SCS) tests, which showed $[H_2O]$ to influence resistance ratio methane characterisation, although this effect's importance depends on the reference gas. Three SCS tests were also performed with gaps of 137 days followed by 295 days, all under similar environmental conditions and gas blends. $[CH_4]$ resistance ratio response changed significantly during the first time gap, suggesting that something inherently changed sensor behaviour, but negligibly during the second time gap, suggesting that natural ageing is not otherwise a key driver of sensor behaviour. Additional SCS tests showed persistent changes in $[CH_4]$ resistance ratio response following hydrogen sulphide exposure; this may have caused a change between controlled SCS tests conducted 137 days apart, although other atmospheric species may also have been responsible. This is an important consideration for laboratory testing and final sensor application. Meanwhile, power loss and sampling dry air negligibly affected a different TGS. In addition, a total of 147 successful sensor characterisation in ambient air (SCA) tests occurred irregularly over approximately 25 months, where small amounts of gas with a high $[CH_4]$ were blended with ambient outdoor air. SCA tests showed a weaker correlation between time and $[CH_4]$ response when restricted to the period covering the second (295-day) time window between the similar SCS tests. A residual observed SCA testing correlation with time could be attributed to changes in $[H_2O]$ over time, supporting SCS testing conclusions.

Received 9th April 2025
Accepted 16th August 2025

DOI: 10.1039/d5ea00046g

rsc.li/esatmospheres

Environmental significance

Temporal changes in the methane response of the semiconductor-based Taguchi Gas Sensor (TGS) were characterised by conducting various characterisation tests in synthetic and ambient air, to understand TGS stability for field applications. Methane sensitivity was characterised using the ratio between measured resistance and a reference resistance, representative of sampling a reference gas. While natural ageing was not observed, exposure to certain atmospheric species caused persistent changes in the methane response. Water also affected sensor behaviour in this resistance ratio approach, although the importance of this under ambient conditions may be small. This means that the TGS can be used for extended autonomous deployment, although caution has to be taken to avoid extreme or prolonged exposure to certain atmospheric species.

1. Introduction

Methane is a potent greenhouse gas with many facility-scale anthropogenic sources such as gas extraction infrastructure, coal mines, landfill sites, wastewater treatment plants and agricultural facilities.[1–3] In order to improve our understanding of facility-scale emissions, downwind *in situ* methane mole

[a]*Laboratoire des Sciences du Climat et de l'Environnement (CEA-CNRS-UVSQ), Institut Pierre-Simon Laplace, Université Paris-Saclay, CEA Saclay, Bâtiment 714, Site de l'Orme des Merisiers, 91191 Gif-sur-Yvette, France. E-mail: adil.shah@lsce.ipsl.fr*
[b]*SUEZ Air & Climate, 15-27 Rue de Port, 92000 Nanterre, France*

fraction ([CH_4]) measurements are required,[4–7] with sufficient accuracy and resolution to detect [CH_4] enhancements above ambient baseline [CH_4] levels, depending on the sampling circumstances (*e.g.* distance from the source or magnitude of emission flux). These measurements can be used to derive top-down (atmospheric measurement-based) flux estimates, which are vital to constrain and verify bottom-up (inventory-based) flux estimates.[8–10] Yet, most high-precision methane sensors are costly, using expensive optical detection methods such as infrared spectroscopy.[11,12] There is an urgent need for cheaper alternatives to complement more precise [CH_4] measurement techniques.[13,14]

Semiconductor-based metal oxide (SMO) sensors are a popular low-cost [CH_4] measurement option. These sensors operate under a potential difference, responding to reducing gases through a change in sensor resistance.[15–17] Oxygen from the atmosphere adsorbs onto the SMO surface by extracting electrons from the bulk material (for n-type sensors), leading to an initial heightened resistance.[18–20] Reducing gases then readily react with this activated oxygen, releasing electrons back into the bulk SMO material, therefore leading to a resistance drop.[15,21] Most n-type SMO sensors contain tin oxide,[15,21,22] to which additives can be introduced to refine sensitivity and selectivity.[13,19,23] Figaro Engineering, Inc. (Osaka, Japan) is a popular SMO sensor manufacturer. Their well-established Taguchi Gas Sensor (TGS) range uses packed grains of tin oxide,[20] sintered onto an alumina substrate,[15] and has been tested in numerous previous studies throughout the years,[17,24–31] with many examples of final application to derive [CH_4][32–39] and even subsequent [CH_4] utilisation in methane flux quantification.[40–43] A vast multitude of [CH_4] derivation approaches has been implemented, using raw measured TGS resistance in conjunction with other environmental measurements, ranging from deterministic models[25,34,35,40,44–46] to machine learning approaches.[33,36,43,47–50]

TGS resistance is influenced by environmental variables, including temperature and humidity,[20] with environmental variables in this manuscript referring to conditions other than dry gas composition. To account for environmental conditions, [CH_4] can be characterised using a reference resistance (R_r), representative of sampling in a certain set of environmental conditions, where R_r is specific to a certain reference methane mole fraction ([CH_4]$_r$) level as well as the overall dry background gas composition (exclusive of [CH_4]).[51] The ratio between measured resistance during a methane mole fraction enhancement (Δ[CH_4]) above [CH_4]$_r$ (obtained under the same environmental conditions and with the same background gas composition as when measuring R_r) and R_r can be used to characterise changes in [CH_4].[24,28,38,52] A power-type fit can model resistance ratio decrease as a function of [CH_4],[24,51] although linear fitting has also been tested in previous work for certain [CH_4] sampling ranges.[31] Inverting the resistance ratio fit therefore allows unknown [CH_4] to be derived.[53] This resistance ratio approach is thought to be independent of environmental effects, with the influence of such effects incorporated into both the numerator and denominator of a resistance ratio,[31,53] allowing for independent [CH_4] TGS characterisation.[15,54] We base this assertion on observations from Jørgensen *et al.*,[52] who observed similar responses for resistance ratio [CH_4] characterisation tests conducted under different environmental conditions, but all with the same background gas composition. Therefore, a [CH_4] resistance ratio characterisation derived at one fixed water mole fraction ([H_2O]) level is thought to be applicable at any other [H_2O] level.[53] However, Jørgensen *et al.*[52] did not observe perfect resistance ratio agreement, and Clifford and Tuma[24] observed variability in gas characterisation fitting with extreme temperature variability. It is important to thoroughly test the assumption of independence of resistance ratio characterisation from environmental variables to improve our understanding of the limitations of this approach, which is a key objective of this work.

While the focus of this work is methane, the independent effect of changes in other reducing gas mole fractions can also be characterised using resistance ratios.[24,38,53] Furthermore, it is possible to derive a single target reducing gas mole fraction, even if other reducing gases vary from their R_r reference gas mole fraction levels during gas characterisation testing, provided that each varying reducing gas mole fraction is independently measured for its effects on resistance ratio to be characterised.[15,24,55] In addition to characterising direct effects on TGS resistance ratio,[15,53] this characterisation must also consider interdependence effects that can occur between each pair of reducing gases varying from their R_r reference gas mole fraction levels.[55] These potential interdependence effects are a reason why reducing gas resistance ratio characterisation testing conducted with a certain background gas composition (exclusive of characterised reducing gases) cannot necessarily be applied to derive an unknown mole fraction from sampling conducted with a different background gas composition, as uncharacterised interdependence effects do not automatically cancel out in a resistance ratio.[55] For example, a [CH_4] resistance ratio characterisation conducted with a carbon monoxide mole fraction ([CO]) of 0 ppm is invalid when applied to sampling conducted with a non-zero [CO], as there is a known interdependence effect between methane and carbon monoxide for the TGS 2611-C00 and TGS 2611-E00, which does not cancel out in resistance ratios.[55] These interdependence effects may explain why resistance ratio gas characterisation fits obtained in ambient air are different from those obtained using synthetic air as a reference gas,[24,28,52] with ambient air affecting TGS resistance exclusive of the effect of methane and carbon monoxide (the dominant reducing gases in ambient air), though the cause of this is unclear.[51,53] Yet, different samples of ambient air (obtained away from sources of reducing gases) appear to have a similar effect on TGS resistance;[51,53] this allows an ambient resistance ratio gas characterisation to be applicable to and comparable to ambient air sampling performed elsewhere or at a different time. This assumes background gas composition to remain the same in different ambient air sources.

A specific fixed background gas composition with a fixed [CH_4]$_r$ should result in a consistent R_r level. Yet, the magnitude of R_r can vary under different environmental conditions, despite

keeping the gas composition fixed.[51] Such environmental effects may be assumed to cancel within a resistance ratio, as discussed above. A variable R_r may be derived for a range of environmental conditions expected during field sampling as a function of measurements, including [H_2O] and temperature, all with the same background gas composition,[28,51] but there may also be a temporal element to R_r due to long-term or short-term drifts in other unidentified factors influencing sensor behaviour.[31,53] The use of a dynamic R_r is a key requirement for optimal application of this resistance ratio [CH_4] characterisation method to capture environmental variability when deriving [CH_4],[31,40] as opposed to other techniques using a static R_r within a resistance ratio.[34,39,44,47] However, Jørgensen *et al.*[52] demonstrated a successful exception by using a static R_r that was able to incorporate environmental effects into resistance ratios, due to sampling under stable outdoor environmental conditions.

It has been suggested in past work that TGS reducing gas sensitivity can drift in general,[26,27,29,34,35,45] though this may be minor.[47,49] While drift in R_r has been previously characterised,[31,53] drift in TGS gas sensitivity has never been tested for the resistance ratio approach described above (independent of environmental effects and background gas composition). Drift in R_r is not necessarily an issue when deriving [CH_4] from resistance ratio, if the change in R_r over time is directly proportional to the change in measured resistance at a certain enhanced [CH_4] level over time (provided correct R_r values are used). This would allow the same resistance ratio [CH_4] characterisation to be used over time, even if R_r varies. However, if the resistance ratio characterisation fit itself drifts, the importance of this resistance ratio variability must be quantified to evaluate its importance when applied to the final sensor application to derive unknown [CH_4]. When considering drift in TGS behaviour over time, it is useful to distinguish between natural sensor ageing due to continuous ambient use and abrupt changes due to specific events.[27,29,31] For example, permanent SMO sensor damage (and hence drifts in TGS sensitivity) may be caused following high exposure to certain atmospheric species.[20,38,56]

In this manuscript, we seek to understand the effect of natural ageing on TGS methane response, as well as the causes of other effects influencing TGS [CH_4] sensitivity. We conducted multiple methane gas characterisation tests under different conditions and at different times to quantify changes in resistance ratio [CH_4] characterisation fits. We present two logging systems in Section 2, where we describe our laboratory testing procedure. Section 2 describes automatic sensor characterisation in ambient air (SCA) tests, where the [CH_4] level was enhanced in an ambient outdoor air gas stream, and sensor characterisation in synthetic air (SCS) tests, where highly regulated synthetic gas blends were sampled. We also describe our analysis method to evaluate changes in TGS sensitivity using resistance ratios in Section 2, where R_r was derived from [CH_4]$_r$ sampling during each test. The results from SCS tests are presented in Section 3, where temporal evolution, dry exposure, power loss, gas exposure and the water effect on TGS methane response are all individually evaluated. Section 4 presents results from SCA tests, where the correlation between TGS methane response and several testing variables (including time) is evaluated, for both the full dataset and a reduced subset assumed to contain no inherent change in TGS behaviour. The outcomes from this work are discussed in Section 5 in the context of their importance in a final TGS application to derive unknown gas mole fractions. We propose the key cause of changes in TGS methane response in Section 6, based on a summary of the results from this work.

2. Experimental methods

2.1. Logging systems

Two logging systems were used during testing. Logger A uses a 0.1 dm^3 glass and stainless-steel cell containing one TGS 2600, one TGS 2611-C00 and two TGS 2611-E00. The two TGS 2611-E00 units are from different batches purchased from different suppliers (labelled TGS 2611-E00 A and TGS 2611-E00 B). TGS 2600, TGS 2611-C00 and TGS 2611-E00 B were first operated in 2018, while TGS 2611-E00 A was first operated in 2021. All of the sensors were operated discontinuously prior to the data presented in this manuscript. Nevertheless, we approximate that TGS 2611-E00 A is at least three years younger than the other sensors in Logger A, in terms of operating time. Logger B uses a 0.1 dm^3 glass and stainless-steel cell containing one TGS 2611-E00 (labelled TGS 2611-E00 C), which was first operated in 2021 (but used rarely).

A 5 V power supply was applied to each TGS, which were each connected in series with a load resistor in both logging systems. Further details of the logging systems are provided in Section S1 of the electronic SI. The voltage drop across each load resistor, as well as the power supply voltage (V_s), was measured at 1 Hz, as described in Section S1 in the SI. This was used to derive 1 Hz resistance measurements for each TGS. Both logging cells contain a temperature and relative humidity sensor (SHT85, Sensirion AG, Staefa, Switzerland), whose measurements were also recorded at 1 Hz.

The Logger A cell was placed in an enclosure with a fan for cell cooling, which was occasionally adjusted in speed or switched off. The Logger B cell had no outer enclosure and was externally exposed to the open laboratory. All SCA tests and SCS tests (see next subsections for details) presented in this manuscript were conducted in an indoor ambient laboratory. For the full period of tests presented in this manuscript, each logger was operated almost continuously (separate periods for each logger), with occasional power loss of no longer than approximately 1 day due to mains power cuts or technical issues. The logging systems did not leave our laboratory building for the full duration of logger testing. A timeline of all recorded successful SCA tests and SCS tests is provided in Fig. 1. Both TGS logging systems were occasionally exposed to various gas mixtures outside of the testing periods presented in this manuscript. This includes undocumented testing or sampling ambient laboratory air, with various operations taking place in this shared laboratory environment. The composition of all sampled gas is not known, although it should be noted that no gas exposure to the TGS loggers was at levels unsafe for human respiration.

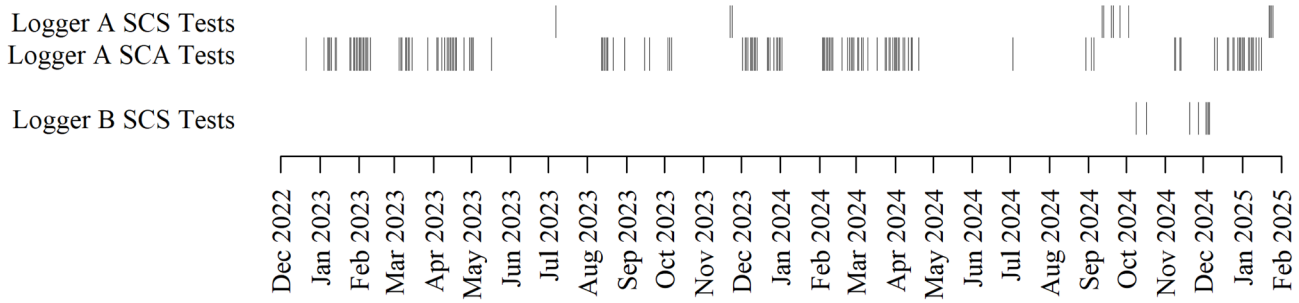

Fig. 1 A timeline of all successful SCS tests and SCA tests presented in this manuscript. The times plotted show the time corresponding to the first data point used to derive the R_r fit for each test.

During testing, a Picarro G2401 (Picarro Inc., Santa Clara, California, USA) gas analyser was placed downstream of the operating logger to sample the same gas passing over each TGS. The Picarro G2401 measures [CH_4], [CO] and [H_2O] with high precision.[57] Picarro G2401 measurements were streamed to each TGS logging system, with the interpolation procedure to adjust the Picarro G2401 data to the TGS timestamp described in Section S2 in the SI.

2.2. Sensor characterisation in the synthetic air testing procedure

Logger A and Logger B were used to conduct three types of controlled SCS tests, as summarised in Table 1. Each test type was conducted from a specific targeted $[CH_4]_r$ level across a [CH_4] range up to a targeted maximum $\Delta[CH_4]$ above $[CH_4]_r$, all with a synthetic background gas composition. These tests were used to evaluate temporal evolution, dry exposure, power loss, gas exposure and the water effect on TGS behaviour, which were characterised using resistance ratios. A list of all completed tests is provided in Section S3 in the SI, along with average observed environmental conditions from each test. Descriptions and justifications of each analysis are provided in Section 3, alongside gas characterisation results. In each test, gas from two sources was blended using mass-flow controllers (EL-FLOW Select, Bronkhorst High-Tech B. V., AK Ruurlo, Netherlands), with an overall constant flow rate to the cell of 1.5 $dm^3\ min^{-1}$. All components were connected using a combination of either stainless-steel tubing or Synflex 1300 tubing (Eaton Corporation plc, Dublin, Ireland), in conjunction with standard stainless-steel Swagelok fittings (Swagelok Company, Solon, Ohio, USA). A chemical scrubber (Sofnocat 514, Molecular Products, Limited, Harlow, Essex, UK) was used during each test to remove residual carbon monoxide present in either of the two sources sampled during blending. A detailed description of the flow set-up for SCS tests is provided in Section S4 in the SI.

The TGS requires many hours to stabilise in response to changes in [H_2O].[50,51] Therefore, all gas was passed through a dew-point generator (LI-610, LI-COR, Inc., Lincoln, Nebraska, USA), which was set to a fixed dew-point setting specific to each test (see Section 3 for details), with gas sampled at the same dew-point setting at least 24 hours before the start of each test. The dew-point generator results in a relatively stable [H_2O] level at a fixed dew point under ambient atmospheric conditions, although [H_2O] is also a function of atmospheric pressure at a fixed dew point temperature, which can cause minor variability. The efficacy of the dew-point generator may also vary gradually over time. Any [H_2O] variability was recorded by the downstream Picarro G2401 (see Section S3 in the SI).

At the start of each of the three test types, the targeted $[CH_4]_r$ level (see Table 1) was sampled for 60 minutes. Then, each of thirteen $\Delta[CH_4]$ levels enhanced above $[CH_4]_r$ was sampled in 15-minute steps, by gradually increasing $\Delta[CH_4]$ up to the maximum targeted $\Delta[CH_4]$ level for each test type (see Table 1) and then gradually bringing it back down to $[CH_4]_r$. This was followed by sampling the $[CH_4]_r$ level again for a further 60 minutes. The entire cycle was repeated twice. An example of a SCS test is shown in Fig. 2. For all tests conducted within a certain test type, the same gas sources and mass-flow controller settings were used (see Section S4 in the SI for details). Yet, the final [CH_4] levels actually sampled were subject to mass-flow controller offset errors (see Shah *et al.*,[58] for example), which may have been responsible for some slight variability in Table 1 $[CH_4]_r$ and maximum $\Delta[CH_4]$ levels during each test. The downstream Picarro G2401 therefore provided reliable mole fraction measurements for reference.

During Test Type 1, gas was blended from two synthetic air cylinders (Deuste Gas Solutions GmbH, Schömberg, Germany), one with a [CH_4] of 1.9 ppm and the other with a [CH_4] of 202 ppm, from a targeted $[CH_4]_r$ level of 1.9 ppm up to a maximum $\Delta[CH_4]$ level of 100 ppm. During Test Type 2, gas was blended from a zero-air generator (UHP-300ZA-S, Parker Hannifin Manufacturing Limited, Gateshead, Tyne and Wear, UK) with gas from the synthetic air cylinder with a [CH_4] of 202 ppm, from a targeted $[CH_4]_r$ of 0.5 ppm up to a maximum $\Delta[CH_4]$ level of 11 ppm. The zero-air generator was supplied with

Table 1 Targeted $[CH_4]_r$ and maximum $\Delta[CH_4]$ levels for each SCS test type

Test type	$[CH_4]_r$ (ppm)	Maximum $\Delta[CH_4]$ (ppm)
Test Type 1	1.9	100
Test Type 2	0.5	11
Test Type 3	0.0	110

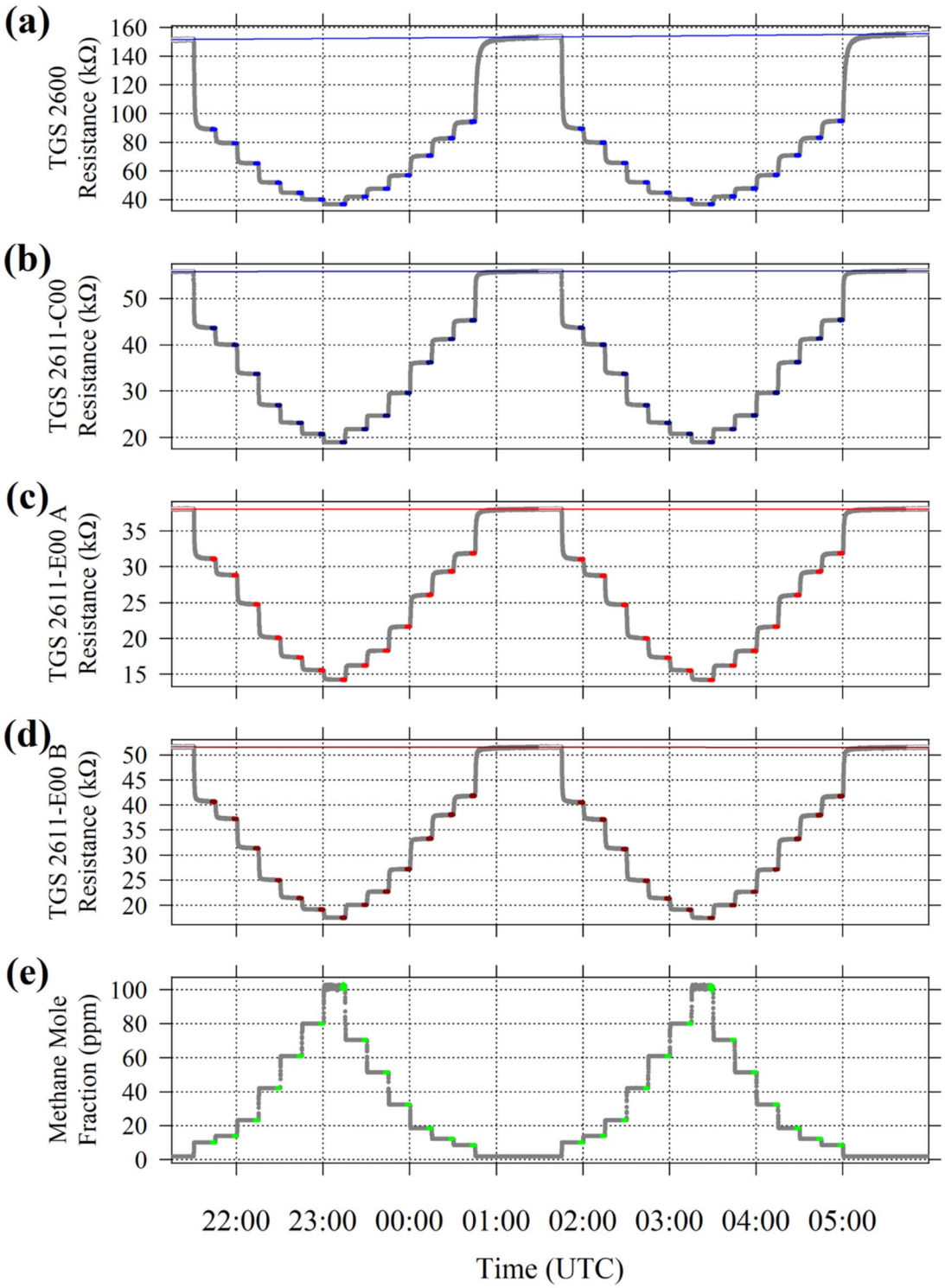

Fig. 2 (a) TGS 2600 resistance, (b) TGS 2611-C00 resistance, (c) TGS 2611-E00 A resistance, (d) TGS 2611-E00 B resistance and (e) Picarro G2401 dry calibrated [CH_4] measurements made during the Test Type 1 SCS temporal evolution test conducted using Logger A in November 2023, plotted as grey dots. 2-Minute averaging periods used to derive $R_{average}$ values are highlighted as coloured dots in (a)–(d) and 2-minute averaging periods used to derive [CH_4] average values are highlighted as coloured dots in (e). Periods used to derive R_r are shown as white-highlighted dots in (a)–(d), over which corresponding second-order polynomial fits are plotted as coloured lines.

compressed outdoor air as input (meaning it was dry and depleted in carbon dioxide compared to ambient conditions); for the purposes of this work, its output gas stream is considered as a type of synthetic air, as it has a similar effect on TGS resistance, as observed in previous work.[51] During Test Type 3 the same gas sources as in Test Type 2 were blended, but

from a targeted $[CH_4]_r$ of 0.0 ppm up to a maximum $\Delta[CH_4]$ level of 110 ppm. Each synthetic air cylinder (Deuste Gas Solutions GmbH) used in this work contains a natural balance of nitrogen, oxygen and argon, with traces of carbon monoxide (less than 1 ppm), carbon dioxide (less than 500 ppm) and nitrous oxide (less than 500 ppb).

In order to obtain continuous R_r values for each test (to subsequently derive resistance ratios), a R_r model was derived by applying a second-order polynomial fit (as a function of time) to measured TGS resistance values obtained during 15 minutes towards the end of each 60-minute $[CH_4]_r$ sampling period. Thus, each TGS resistance measurement has a corresponding R_r level. The duration of each test is defined as the interval from the time of the first data point up until the time of the final data point used to derive R_r fits. For each 15-minute enhanced $[CH_4]$ sampling period, a 2-minute resistance ratio average ($RR_{average}$) between measured resistance (the numerator) and corresponding R_r values (the denominator) was taken from towards the end of the 15-minute interval. The time of the first data point used to derive each R_r fit is plotted in Fig. 1 for each Logger A and Logger B SCS test (see Section S3 in the SI for start time strings).

Periods for R_r derivation and averaging periods used to derive each $RR_{average}$ value (during $[CH_4]$ enhancements) were chosen to be sufficiently long to capture short-term noise during stable sampling. Yet a sufficient time duration prior to these periods was also required to enable the sensors to stabilise to the latest $[CH_4]$ change. This was the case for most of the sensors, as illustrated in Fig. 2, where each sensor typically had enough time to reach a stable resistance level before data were used for averaging or for producing a R_r model fit. However, TGS 2600 exhibited a longer delay in response to $[CH_4]$ changes and did not always perfectly stabilise compared to the other sensors (see Fig. 2 for example). Nevertheless, this averaging approach is a sufficient approximation in this work to analyse changes in sensor behaviour, comparing tests conducted under different conditions or at different times, but all analysed in the same way.

2.3. Sensor characterisation in the ambient air testing procedure

Logger A was used to conduct roughly daily automatic SCA tests between 21 December 2022 and 16 January 2025, subject to the availability of both the TGS logging system and the Picarro G2401, with the test start time shifting throughout the day. Wet outdoor air with an ambient background gas composition was pumped into a gas stream at approximately (6 ± 1) dm^3 min^{-1}. Following 60 minutes of pure ambient outdoor air sampling for each test, small quantities of gas from an argon cylinder (Air Products SAS, Saint Quentin Fallavier, France) with a $[CH_4]$ of 100 000 ppm were blended into the gas stream in seven 15-minute steps using mass-flow controllers (EL-FLOW Select). All components were connected using a combination of either stainless-steel tubing or Synflex 1300 tubing (Eaton Corporation plc), in conjunction with standard stainless-steel Swagelok fittings (Swagelok Company). A detailed description of the flow set-up for SCA tests is provided in Section S5 in the SI. Each enhanced $[CH_4]$ sampling step was followed by sampling pure ambient outdoor air for 30 minutes. The final $\Delta[CH_4]$ level was followed by at least 45 minutes of pure ambient outdoor air sampling. The same mass-flow controller sequence was used in each SCA test, although sampled $\Delta[CH_4]$ levels were subject to variations in the flow rate of the pure ambient outdoor air gas stream (which was not regulated), resulting in an average maximum $\Delta[CH_4]$ level of (118 ± 17) ppm. An example of a SCA test is shown in Fig. 3. The flow rate to Logger A was constantly maintained at 1.5 dm^3 min^{-1} using a mass-flow controller (EL-FLOW Select), subsampling from the main gas stream (see Section S5 in the SI for details). During testing, the proportion of gas from the argon cylinder with a $[CH_4]$ of 100 000 ppm contributed no more than 0.2% towards the total gas blend; it can therefore be assumed that changes on the overall gas matrix (including $[H_2O]$) were negligible when sampling $[CH_4]$ enhancements compared to sampling pure ambient outdoor air.

Quality control procedures, which are described in Section S6 in the SI, were applied using measurements made from each test to eliminate unusable or unreliable tests from the final analysis. This resulted in 147 successful SCA tests. For each of these tests, the standard deviation in [CO] was less than $\pm$0.05 ppm and the standard deviation in temperature was less than $\pm$0.2 K for the duration of each test (defined below). The standard deviation in $[H_2O]$ (for periods sampling raw $[CH_4]$ of less than 5 ppm) was less than $\pm$0.1%, for the duration of each test (defined below).

A R_r model (corresponding to sampling pure ambient outdoor air) was derived for each Logger A TGS using 5 minutes of sampling towards the end of each 30-minute pure ambient outdoor air sampling period. This was combined with 10 minutes of pure ambient outdoor air sampling before the first $\Delta[CH_4]$ level and the final 20 minutes (out of 45 minutes) after sampling the final $\Delta[CH_4]$ level. A third-order polynomial fit was applied to these data to derive R_r as a function of time for each TGS for each test. For each R_r fit, its root-mean squared error (RMSE) is no greater than 1% of the average modelled R_r for the full duration of each test. The duration of each test is defined as the interval from the time of the first data point up until the time of the final data point used to derive R_r fits. The time of the first data point used to derive the R_r fit is plotted in Fig. 1 for each SCA test. The standard deviation in $[CH_4]_r$ during all periods used to derive each R_r fit was less than $\pm$0.1 ppm for each SCA test (see next subsection for details on $[CH_4]$). For each 15-minute enhanced $[CH_4]$ sampling period, a 1-minute $RR_{average}$ between measured resistance (the numerator) and corresponding R_r values (the denominator) was taken from towards the end of the interval. As discussed in the previous subsection, the averaging periods used to derive each $RR_{average}$ value in additon to R_r modelling periods were deemed to be sufficiently long to capture short-term noise but with enough time having elapsed from the previous transition for sensor resistances to have stabilised in response to the $[CH_4]$ change (see Fig. 3).

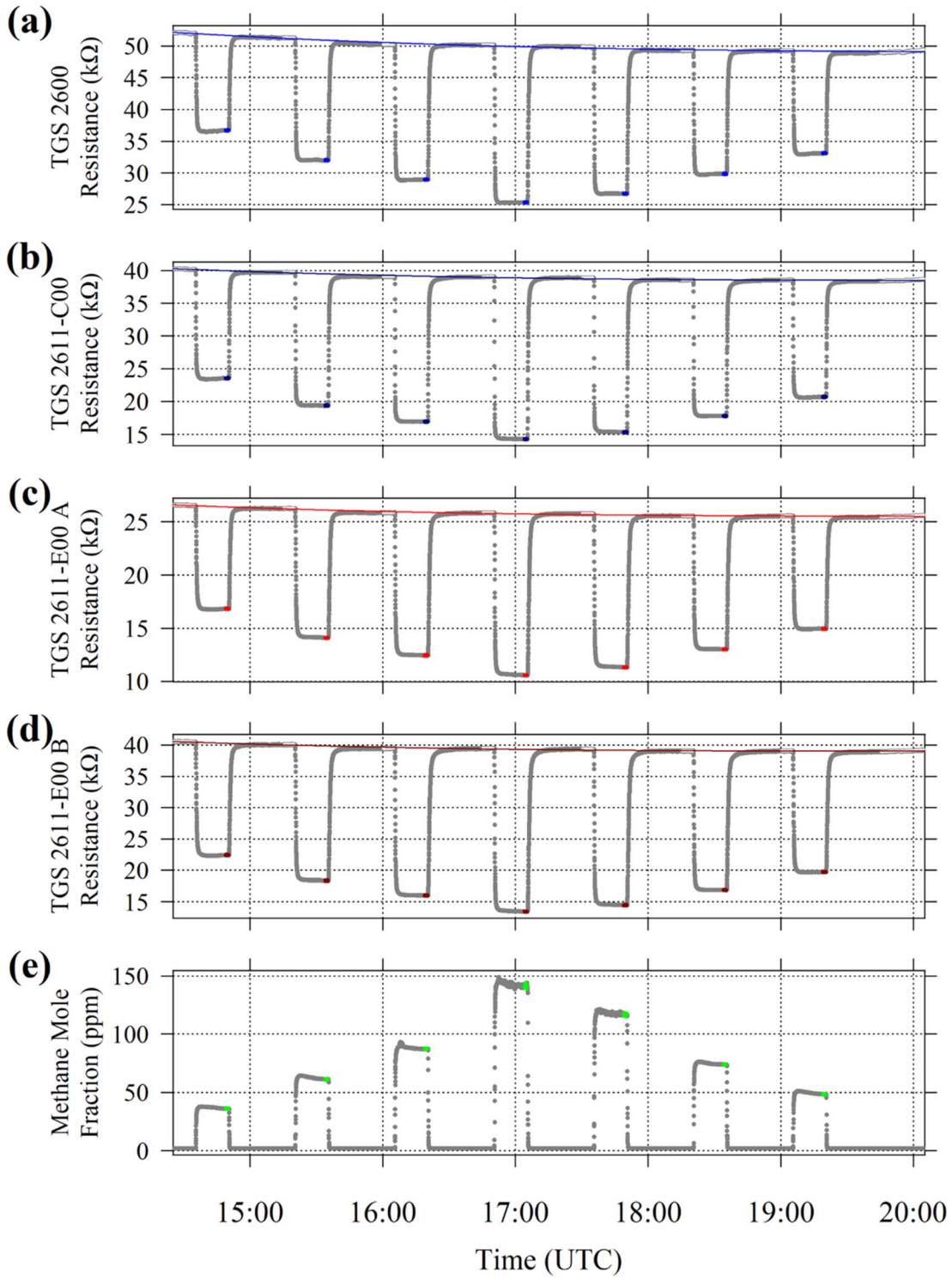

Fig. 3 (a) TGS 2600 resistance, (b) TGS 2611-C00 resistance, (c) TGS 2611-E00 A resistance, (d) TGS 2611-E00 B resistance and (e) Picarro G2401 dry calibrated [CH_4] measurements made during the automatic SCA test conducted using Logger A starting at 14 : 25 : 11 UTC on 18 February 2024, plotted as grey dots. 2-Minute averaging periods used to derive $R_{average}$ values are highlighted as coloured dots in (a)–(d) and 2-minute averaging periods used to derive [CH_4] average values are highlighted as coloured dots in (e). Periods used to derive R_r are shown as white-highlighted dots in (a)–(d), over which corresponding third-order polynomial fits are plotted as coloured lines.

2.4. Methane mole fraction measurements

All raw wet Picarro G2401 [CH_4] measurements were first empirically water-corrected by applying a third-order polynomial water correction using Picarro G2401 reported [H_2O] measurements. Water correction coefficients were initially derived by sampling gas with a fixed [CH_4]

(approximately 2 ppm) and varying [H_2O] to evaluate how raw wet [CH_4] measurements change under wet conditions compared to a measurement of the same gas under dry conditions, as a function of Picarro G2401 reported [H_2O] measurements. However, this correction could not be applied to all Picarro G2401 reported [H_2O] measurements during SCS and SCA testing, as [H_2O] measurements can become unreliable at high [CH_4] levels. This may be because of the close proximity of the methane and water infrared absorption lines used by the Picarro G2401, causing spectral interference at high [CH_4]. Therefore, modelled [H_2O] values were derived from all reported [H_2O] measurements made when raw [CH_4] measurements were less than 5 ppm, for the full duration of each test. For SCS tests, a second-order polynomial fit was applied to raw reported [H_2O] measurements as a function of time to derive modelled reported [H_2O] values. However, a third-order polynomial fit was used to derive modelled reported [H_2O] values for SCA tests, as there was greater [H_2O] variability when sampling ambient outdoor air, as opposed to sampling gas passing through the dew-point generator (LI-610) during SCS tests. Although [H_2O] was relatively stable for SCS tests, this approach nevertheless accounted for minor drift in [H_2O], especially due to the potential impact of pressure variations on the dew-point generator throughout each test. These reported [H_2O] fits were used to produce modelled reported [H_2O] values as a function of time, for the full duration of each test. This allowed a water correction to be applied to all raw wet [CH_4] measurements using either raw reported [H_2O] measurements or modelled reported [H_2O] (when raw wet [CH_4] was greater than 5 ppm).

Then a calibration correction was applied to all corrected dry [CH_4] measurements, for use in the subsequent analysis. Linear calibration coefficients for the Picarro G2401 gas analyser were initially derived by comparing raw wet [CH_4] measurements under dry sampling conditions to reference gas standards on the World Meteorological Organisation greenhouse gas scale for methane (WMO X2004A). Hence, all [CH_4] measurements used in this work represent dry calibrated [CH_4].

A specific $[CH_4]_r$ level was derived for each SCS and SCA test by taking the average of all dry calibrated [CH_4] measurements during each of the periods used to derive each R_r fit. Dry calibrated [CH_4] averages were also derived from the final 2 minutes (for SCS tests) or 1 minute (for SCA tests) of each 15-minute enhanced [CH_4] sampling period, corresponding to each averaging period used to derive $RR_{average}$ values. The differences between each [CH_4] average and the overall average $[CH_4]_r$ level from each test were used as $\Delta[CH_4]$ values in the subsequent analysis.

2.5. Gas characterisation analysis

For each SCS test and SCA test, TGS response was characterised using $\Delta[CH_4]$ values and corresponding $RR_{average}$ values using

$$RR_{average} = \left(1 + \left(\frac{\Delta[CH_4]}{m}\right)\right)^{-\mu}, \quad (1)$$

to derive a characteristic methane mole fraction (m) and a methane power (μ). This modified power fit is adapted from Shah *et al.*,[51] for a single gas, and is similar to the approach of Clifford and Tuma,[24] who instead used [CH_4] in place of $\Delta[CH_4]$. $RR_{average}$ is typically limited to between zero and one; it can only exceed one if the average measured resistance is greater than R_r, which is not expected unless [CH_4] is lower than $[CH_4]_r$.

Eqn (1) can be inverted to derive $\Delta[CH_4]$ as a function of a certain specific pre-defined resistance ratio in place of $RR_{average}$, by making $\Delta[CH_4]$ the subject. This allows for the evaluation of the change in $\Delta[CH_4]$ estimation between different tests using a consistent metric (*i.e.* a fixed resistance ratio). The choice of pre-defined fixed resistance ratio to derive corresponding $\Delta[CH_4]$ eqn (1) output can be adjusted to ideally intersect with the measured $RR_{average}$ range. It should be noted that eqn (1) $\Delta[CH_4]$ input is derived from dry calibrated [CH_4] measurements made by the Picarro G2401. Hence, any derived $\Delta[CH_4]$ output also represents a dry calibrated value.

It is important to note here that tests conducted with different $[CH_4]_r$ levels are not comparable, as a higher $[CH_4]_r$ level has a direct effect of lowering the starting R_r level, resulting in a different gas characterisation fit. In addition, tests conducted with a different dry background gas composition (exclusive of [CH_4]) are also not comparable, due to potential interdependence effects,[55] as discussed in Section 1. This means that coefficients derived with an ambient background gas composition cannot be directly compared to those derived with a synthetic background gas composition, even if $[CH_4]_r$ remains the same in both tests.[53] Similarly, coefficients derived with a $[CH_4]_r$ level of 2 ppm cannot be directly compared to those derived with a $[CH_4]_r$ level of 0 ppm, even if both tests were conducted with the same synthetic background gas composition. Thus, in this work, results from SCS tests can only be compared to results from other SCS tests of the same test type (each SCS test type has a different $[CH_4]_r$ level), and results from SCA tests can only be compared to results from other SCA tests. Comparing between different SCA tests assumes that there was no major change in overall ambient air background gas composition, which is a reasonable assumption considering that all outdoor ambient air was sampled from the same semi-rural location of our laboratory.

3. Sensor characterisation in synthetic air analysis and results

3.1. Temporal evolution test

As discussed in Section 1, TGS sensitivity may evolve over time either due to natural sensor ageing or due to discrete events causing long-term persistent changes. The use of precise resistance ratio gas characterisation curves allows for a robust analysis of such effects.[54] Logger A was used to conduct both Test Type 1 and Test Type 2 temporal evolution tests. Test Type 2 has a much lower $\Delta[CH_4]$ range than Test Type 1 (see Table 1), allowing changes in TGS response to be evaluated under these two different conditions. Test Type 1 was performed on 23 November 2023 and 12 September 2024. Gas characterisation curves for Test Type 1 temporal evolution tests are presented in Fig. 4, with the gas characterisation coefficients, coefficient of

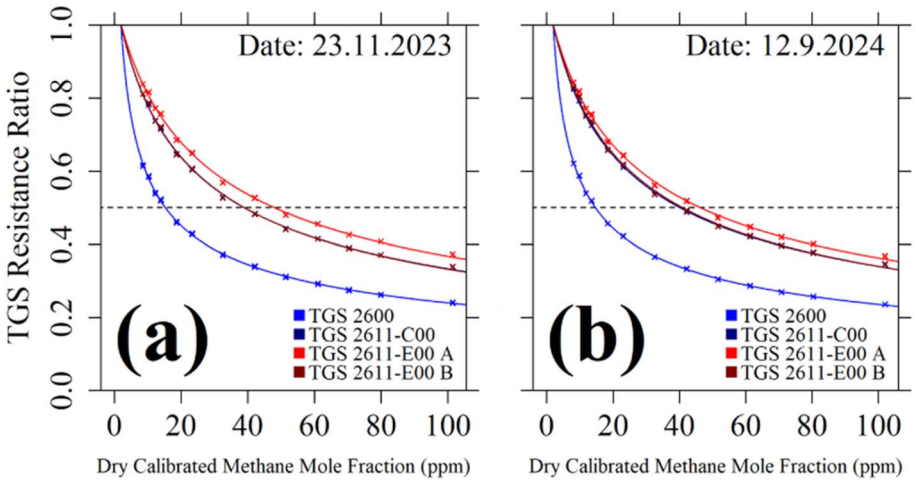

Fig. 4 $RR_{average}$ plotted as a function of [CH_4] as coloured crosses (see legend for colours for each TGS) for Test Type 1 Logger A SCS temporal evolution tests in (a) November 2023 and (b) September 2024. Corresponding eqn (1) model fits are shown as coloured lines. Resistance ratios of 0.5 Ω $Ω^{-1}$ are indicated by vertical dashed lines. Resistance ratio curves for TGS 2611-C00 and TGS 2611-E00 B closely overlap, making them difficult to distinguish. Dates correspond to the time of the first data point used to derive R_r polynomial fits.

Table 2 Gas characterisation coefficients from Test Type 1 Logger A SCS temporal evolution tests with corresponding R^2 and RMSE values. Δ[CH_4]$_{0.5}$ is given for each TGS for each test. The average R_r during periods used to derive R_r polynomial fits is given for each TGS

Sensor	Test month	m (ppm)	μ	R^2	RMSE (mΩ $Ω^{-1}$)	Δ[CH_4]$_{0.5}$ (ppm)	R_r (kΩ)
TGS 2600	November 2023	2.86	0.400	0.9993	±3.29	13.3	153
	September 2024	2.74	0.400	0.9995	±2.84	12.7	157
TGS 2611-C00	November 2023	12.4	0.502	0.9993	±4.32	37.0	55.9
	September 2024	12.6	0.496	0.9994	±4.12	38.3	52.9
TGS 2611-E00 A	November 2023	15.5	0.502	0.9986	±5.88	46.1	38.1
	September 2024	14.6	0.497	0.9985	±6.17	44.5	37.2
TGS 2611-E00 B	November 2023	12.8	0.510	0.9985	±6.17	37.0	51.6
	September 2024	13.6	0.512	0.9985	±6.45	39.0	49.0

determination (R^2) and RMSE of each model fit provided in Table 2, alongside the average R_r during periods used to derive R_r polynomial fits. Test Type 2 was performed on 7 July 2023, 21 November 2023 and 11 September 2024. Gas characterisation resistance ratio curves for Test Type 2 temporal evolution tests are presented in Fig. 5, with the gas characterisation coefficients, R^2 and RMSE of each model fit provided in Table 3, alongside the average R_r during periods used to derive R_r

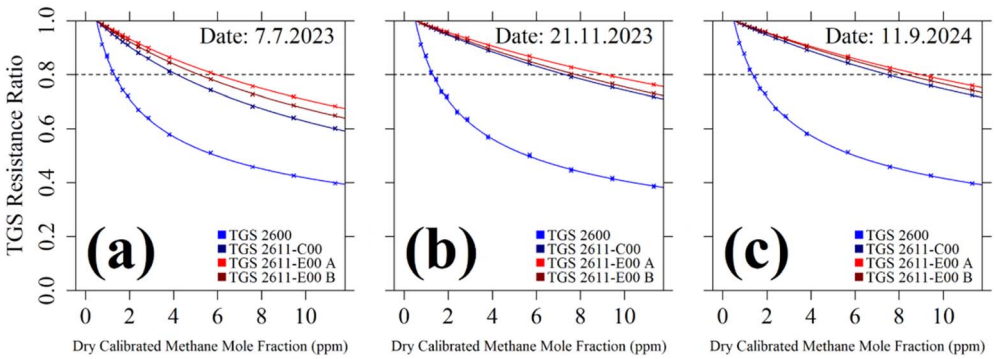

Fig. 5 $RR_{average}$ plotted as a function of [CH_4] as coloured crosses (see legend for colours for each TGS) for Test Type 2 Logger A SCS temporal evolution tests in (a) July 2023, (b) November 2023 and (c) September 2024. Corresponding eqn (1) model fits are shown as coloured lines. Resistance ratios of 0.8 Ω $Ω^{-1}$ are indicated by vertical dashed lines. Dates correspond to the time of the first data point used to derive R_r polynomial fits.

Table 3 Gas characterisation coefficients from Test Type 2 Logger A SCS temporal evolution tests with corresponding R^2 and RMSE values. $\Delta[CH_4]_{0.8}$ is given for each TGS for each test. The average R_r during periods used to derive R_r polynomial fits is given for each TGS

Sensor	Test month	m (ppm)	μ	R^2	RMSE (mΩ Ω^{-1})	$\Delta[CH_4]_{0.8}$ (ppm)	R_r (kΩ)
TGS 2600	July 2023	0.97	0.367	0.9992	±4.66	0.81	154
	November 2023	1.01	0.385	0.9988	±5.73	0.79	224
	September 2024	1.09	0.386	0.9990	±5.38	0.86	220
TGS 2611-C00	July 2023	8.4	0.616	0.9997	±2.26	3.66	55.0
	November 2023	21.9	0.824	0.9998	±1.20	6.80	59.0
	September 2024	21.5	0.794	0.9998	±1.12	6.98	55.7
TGS 2611-E00 A	July 2023	11.7	0.581	0.9998	±1.49	5.47	36.9
	November 2023	23.8	0.722	0.9998	±0.94	8.63	39.9
	September 2024	25.1	0.766	0.9998	±1.18	8.47	38.9
TGS 2611-E00 B	July 2023	11.1	0.637	0.9998	±1.75	4.66	52.0
	November 2023	28.0	0.963	0.9998	±1.32	7.31	54.1
	September 2024	34.0	1.079	0.9997	±1.41	7.81	51.3

polynomial fits. All sampling during Test Type 1 and Test Type 2 temporal evolution tests was conducted with the dew-point generator (LI-610) set to a dew-point setting of 8 °C.

Fig. 4 and 5 allow for visual inspection of the change in TGS methane response over time. To quantify this change in sensor behaviour, modelled methane mole fraction enhancement corresponding to a fixed resistance ratio of 0.5 Ω Ω^{-1} ($\Delta[CH_4]_{0.5}$) was derived for Test Type 1 and modelled methane mole fraction enhancement corresponding to a fixed resistance ratio of 0.8 Ω Ω^{-1} ($\Delta[CH_4]_{0.8}$) was derived for Test Type 2. Different fixed reference resistance ratios were used due to the different resistance ratio ranges observed in each test type. These results are given in Table 2 for Test Type 1 and Table 3 for Test Type 2, which show that the greatest change in sensor behaviour occurred between July 2023 and November 2023 for Test Type 2, for all sensors except TGS 2600. The change in sensor behaviour between November 2023 and September 2024 was relatively small for both Test Type 1 and Test Type 2. For example, Test Type 2 $\Delta[CH_4]_{0.8}$ was 6.80 ppm in November 2023 for TGS 2611-C00, while this increased very slightly in September 2024 to 6.98 ppm. Yet there was a significant difference in July 2023 for Test Type 2, with a $\Delta[CH_4]_{0.8}$ of 3.66 ppm for TGS 2611-C00.

The fact that sensor behaviour did not significantly change for both Test Type 1 and Test Type 2 (which sampled from different $[CH_4]_r$ levels and across different $\Delta[CH_4]$ ranges) between November 2023 and September 2024, suggests that general natural sensor ageing does not have a significant effect on TGS behaviour over a period of almost a year. By contrast, the major change in behaviour between July 2023 and November 2023 for most of the TGSs suggests that something else caused a persistent and abrupt change in sensor response. As noted in Section 2, the logging systems may have sampled certain interfering species. While there is no certainty about which species the loggers were exposed to, possible candidates in our laboratory environment include acetylene, ethane, ethanol and hydrogen sulphide, which may potentially cause abrupt long-term sensor changes. Other plausible possibilities of Test Type 1 and Test Type 2 sensor variability over time include dry

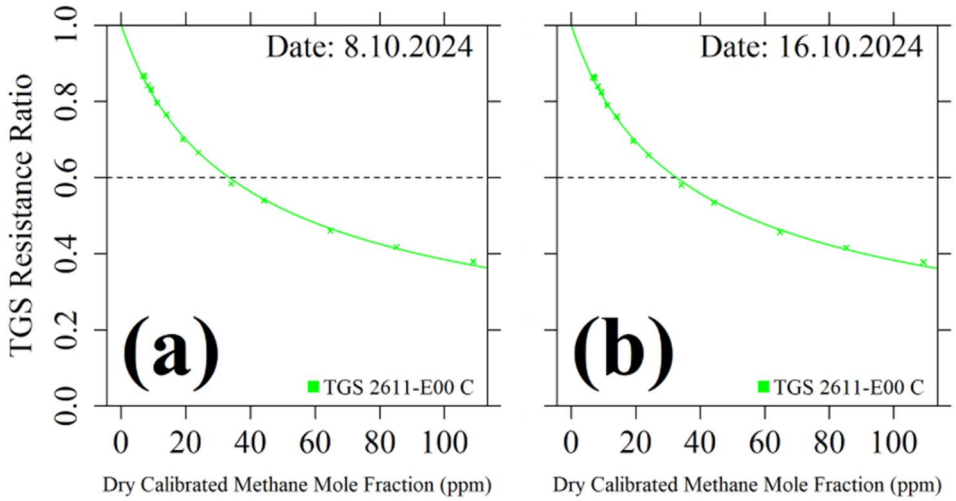

Fig. 6 $RR_{average}$ plotted as a function of $[CH_4]$ as green crosses for Test Type 3 Logger B SCS dry exposure tests: (a) before dry exposure and (b) after dry exposure. Corresponding eqn (1) model fits are shown as green lines. Resistance ratios of 0.6 Ω Ω^{-1} are indicated by vertical dashed lines. Dates correspond to the time of the first data point used to derive R_r polynomial fits.

Table 4 Gas characterisation coefficients from Test Type 3 Logger B SCS dry exposure tests with corresponding R^2 and RMSE values. $\Delta[CH_4]_{0.6}$ is given for each test. The average R_r during periods used to derive R_r polynomial fits is given

Sensor	Test status	m (ppm)	μ	R^2	RMSE (mΩ Ω^{-1})	$\Delta[CH_4]_{0.6}$ (ppm)	R_r (kΩ)
TGS 2611-E00 C	Before dry exposure	23.0	0.569	0.9985	±6.68	33.4	43.9
	After dry exposure	21.5	0.554	0.9985	±6.56	32.6	41.6

sampling and power loss. These ideas are tested in the subsequent subsections.

3.2. Dry exposure test

Although it has been shown that TGS methane response becomes difficult to characterise under dry sampling conditions,[51] the long-term effect of dry exposure on sensor behaviour has not been tested before, to our knowledge. Test Type 3 was therefore conducted using Logger B on 8 October 2024. The logger was then exposed to dry conditions for exactly 48 hours between 9 October 2024 and 11 October 2024, by passing gas from the zero-air generator (UHP-300ZA-S) through a chemical water scrubber, containing magnesium perchlorate grains (10034-81-8, ThermoFisher (Kandel) GmbH, Kandel, Germany). Logger B then sampled pure ambient outdoor air before conducting Test Type 3 again on 16 October 2024. Both tests were performed using the same 8 °C dew-point setting applied to the dew-point generator (LI-610). Gas characterisation resistance ratio curves for Test Type 3 dry exposure tests are presented in Fig. 6, with the gas characterisation coefficients, R^2 and RMSE of each model fit provided in Table 4, alongside the average R_r during periods used to derive R_r polynomial fits.

Average environmental conditions are provided for each SCS test in Section S3 in the SI, which show that almost identical conditions were present during both tests, with an almost identical measured average $[CH_4]_r$ before and after dry exposure. Modelled methane mole fraction enhancement corresponding to a fixed resistance ratio of 0.6 Ω Ω^{-1} ($\Delta[CH_4]_{0.6}$) was used to evaluate changes in sensor behaviour. $\Delta[CH_4]_{0.6}$ changed from 33.4 ppm before dry exposure to 32.6 ppm after dry exposure. This negligible $\Delta[CH_4]_{0.6}$ change suggests that prolonged dry sampling does not significantly affect TGS behaviour, in the context of methane sensitivity, with two full days of dry exposure used for this test.

3.3. Power loss test

The loss of power is known to cause changes in TGS resistance response, although this is thought to be a temporary effect.[15,31] It is therefore useful to verify that long-term persistent changes in TGS methane response do not occur following power loss. This is an important consideration as gas characterisation may take place some time away from final sensor application, during which a power loss is possible, especially during transportation. Power loss can also be caused during field deployment due to mains power cuts or during low solar exposure when using solar power, for example.

Test Type 3 was conducted using Logger B on 19 November 2024. The logger was then exposed to pure ambient outdoor air for 1 hour on 20 November 2024, before being abruptly switched off from the power supply unit for 48 hours with no more air flow (although ambient laboratory air could slowly diffuse into the cell). Logger B was then switched on, and pure ambient outdoor air was sampled for a further 72 hours before sampling gas from the zero-air generator (UHP-300ZA-S). Test Type 3 was

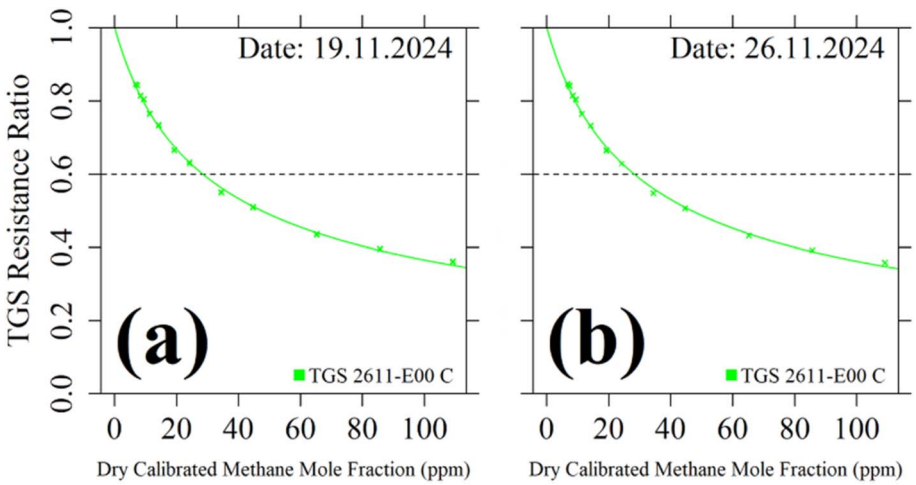

Fig. 7 $RR_{average}$ plotted as a function of $[CH_4]$ as green crosses for Test Type 3 Logger B SCS power loss tests: (a) before power loss and (b) after power loss. Corresponding eqn (1) model fits are shown as green lines. Resistance ratios of 0.6 Ω Ω^{-1} are indicated by vertical dashed lines. Dates correspond to the time of the first data point used to derive R_r polynomial fits.

Table 5 Gas characterisation coefficients from Test Type 3 Logger B SCS power loss tests with corresponding R^2 and RMSE values. $\Delta[CH_4]_{0.6}$ is given for each test. The average R_r during periods used to derive R_r polynomial fits is given

Sensor	Test status	m (ppm)	μ	R^2	RMSE (mΩ Ω^{-1})	$\Delta[CH_4]_{0.6}$ (ppm)	R_r (kΩ)
TGS 2611-E00 C	Before power loss	17.4	0.527	0.9983	±6.92	28.5	42.0
	After power loss	17.7	0.536	0.9984	±6.82	28.2	43.5

then repeated on 26 November 2024. Both tests were performed using the same 8 °C dew-point setting applied to the dew-point generator (LI-610). Gas characterisation resistance ratio curves for Test Type 3 power loss tests are presented in Fig. 7, with the gas characterisation coefficients, R^2 and RMSE of each model fit provided in Table 5, alongside the average R_r during periods used to derive R_r polynomial fits. Changes in sensor behaviour were evaluated using $\Delta[CH_4]_{0.6}$. As gas characterisation coefficients derived both before and after power loss are almost identical, with similar $\Delta[CH_4]_{0.6}$ results, this suggests that the simple loss of power does not have a significant long-term effect on TGS methane response.

3.4. Gas exposure test

As discussed in Section 1, excessive or prolonged TGS exposure to certain atmospheric species (either in the field or the laboratory) may cause changes in sensor behaviour. It is possible that the gases present in our testing laboratory may have influenced TGS behaviour. Therefore, the effect of exposure to three reducing gases was tested, namely ethane, hydrogen sulphide and acetylene. Test Type 3 was performed four times using Logger B roughly one day apart, with 2 hours of exposure to each gas between each test (with Test Type 3 conducted at least three hours after the end of gas exposure), all with the dew-point generator (LI-610) set to the same 8 °C dew-point setting. Ethane exposure was conducted by sampling gas from a synthetic air cylinder (Deuste Gas Solutions GmbH) with an ethane mole fraction of approximately 50 ppm (and a $[CH_4]$ of 2 ppm) at 0.5 dm^3 min^{-1}. Hydrogen sulphide exposure was conducted by sampling gas from a synthetic air cylinder (Deuste Gas Solutions GmbH) with a hydrogen sulphide mole fraction of approximately 10 ppm (and a $[CH_4]$ of 2 ppm) at 0.5 dm^3 min^{-1}. Acetylene exposure was conducted by sampling a blend of gas from the zero-air generator (UHP-300ZA-S) and gas from an argon cylinder (Air Products N.V., Diegem, Belgium) with an acetylene mole fraction of 10 ppm, targeting an acetylene mole fraction of approximately 1 ppm, at 1.5 dm^3 min^{-1}. The same procedure was repeated using Logger A, but the order of gas exposure was reversed.

Gas characterisation resistance ratio curves for Test Type 3 gas exposure tests are presented in Fig. 8 for Logger B and Fig. 9 for Logger A, with the gas characterisation coefficients, R^2 and RMSE of each model fit provided in Table 6 for Logger B and Table 7 for Logger A, alongside the average R_r during periods used to derive R_r polynomial fits. $\Delta[CH_4]_{0.6}$ is given in Table 6 for Logger B testing, and modelled methane mole fraction enhancement corresponding to a fixed resistance ratio of 0.4 Ω Ω^{-1} ($\Delta[CH_4]_{0.4}$) is given in Table 7 for Logger A testing. These $\Delta[CH_4]_{0.6}$ and $\Delta[CH_4]_{0.4}$ results show that hydrogen sulphide has a clear and pronounced persistent impact on sensor behaviour, as observed elsewhere,[38] with TGS 2611-C00 $\Delta[CH_4]_{0.4}$ decreasing in this work from 53.7 ppm to 23.1 ppm, for example. The effect due to hydrogen sulphide is less pronounced (but still significant) for the three tested TGS 2611-E00 units, which may be because a filter is integrated within these sensors, although it is difficult to draw any definite conclusions due to the small sample size. There also appears to be a small change in sensor behaviour following Logger A ethane exposure. However, no effect is observed following Logger B ethane exposure. This Logger A ethane effect may be a residual effect of hydrogen sulphide, rather than that of

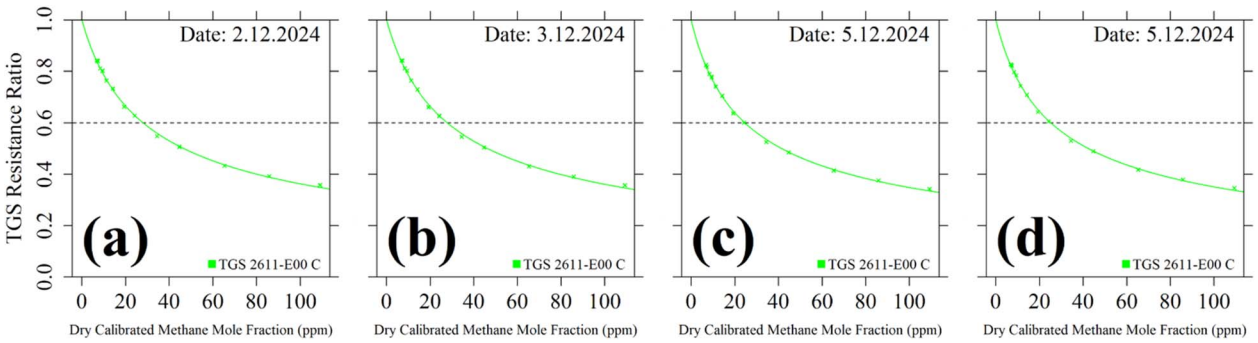

Fig. 8 $RR_{average}$ plotted as a function of $[CH_4]$ as green crosses for Test Type 3 Logger B SCS gas exposure tests: (a) before gas exposure, (b) after exposure to an ethane mole fraction of 50 ppm, (c) after exposure to a hydrogen sulphide mole fraction of 10 ppm and (d) after exposure to an acetylene mole fraction of 1 ppm. Corresponding eqn (1) model fits are shown as green lines. Resistance ratios of 0.6 Ω Ω^{-1} are indicated by vertical dashed lines. Dates correspond to the time of the first data point used to derive R_r polynomial fits.

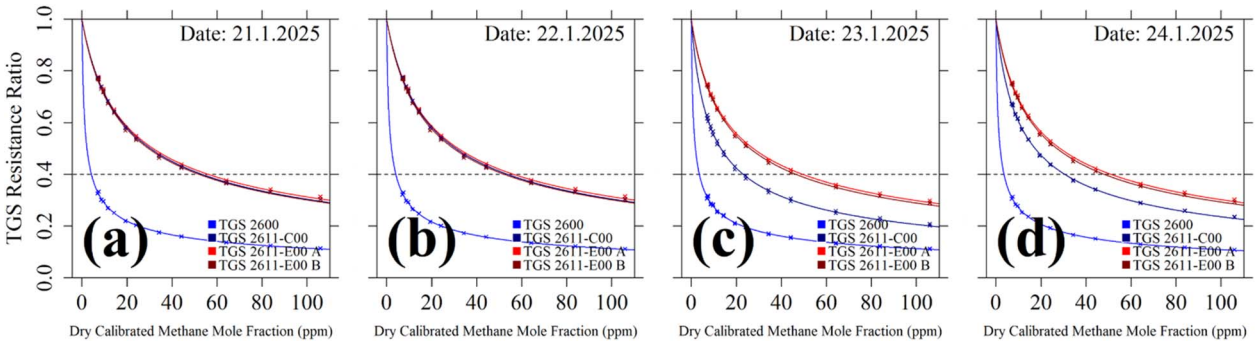

Fig. 9 $RR_{average}$ plotted as a function of $[CH_4]$ as coloured crosses (see legend for colours for each TGS) for Test Type 3 Logger A SCS gas exposure tests: (a) before gas exposure, (b) after exposure to an acetylene mole fraction of 1 ppm, (c) after exposure to a hydrogen sulphide mole fraction of 10 ppm and (d) after exposure to an ethane mole fraction of 50 ppm. Corresponding eqn (1) model fits are shown as coloured lines. Resistance ratios of 0.4 $\Omega\ \Omega^{-1}$ are indicated by vertical dashed lines. Dates correspond to the time of the first data point used to derive R_r polynomial fits.

Table 6 Gas characterisation coefficients from Test Type 3 Logger B SCS gas exposure tests with corresponding R^2 and RMSE values. $\Delta[CH_4]_{0.6}$ is given for each test. The average R_r during periods used to derive R_r polynomial fits is given

Sensor	Test status	m (ppm)	μ	R^2	RMSE (m$\Omega\ \Omega^{-1}$)	$\Delta[CH_4]_{0.6}$ (ppm)	R_r (kΩ)
TGS 2611-E00 C	Before gas exposure	17.3	0.530	0.9985	±6.46	28.0	43.1
	After exposure to ethane	17.3	0.533	0.9983	±7.00	27.9	43.3
	After exposure to hydrogen sulphide	13.9	0.502	0.9989	±5.44	24.6	42.8
	After exposure to acetylene	14.6	0.508	0.9987	±6.03	25.3	42.7

Table 7 Gas characterisation coefficients from Test Type 3 Logger A SCS gas exposure tests with corresponding R^2 and RMSE values. $\Delta[CH_4]_{0.4}$ is given for each test. The average R_r during periods used to derive R_r polynomial fits is given for each TGS

Sensor	Test status	m (ppm)	μ	R^2	RMSE (m$\Omega\ \Omega^{-1}$)	$\Delta[CH_4]_{0.4}$ (ppm)	R_r (kΩ)
TGS 2600	Before gas exposure	0.507	0.410	0.9973	±3.90	4.2	307
	After exposure to acetylene	0.496	0.412	0.9969	±4.16	4.1	313
	After exposure to hydrogen sulphide	0.383	0.392	0.9960	±4.41	3.6	229
	After exposure to ethane	0.412	0.404	0.9969	±3.90	3.6	276
TGS 2611-C00	Before gas exposure	10.20	0.501	0.9989	±5.31	53.4	55.1
	After exposure to acetylene	10.35	0.503	0.9989	±5.41	53.7	55.1
	After exposure to hydrogen sulphide	4.32	0.496	0.9980	±6.46	23.1	51.7
	After exposure to ethane	5.66	0.494	0.9991	±4.53	30.5	52.7
TGS 2611-E00 A	Before gas exposure	9.85	0.482	0.9983	±6.58	56.0	39.6
	After exposure to acetylene	9.94	0.483	0.9983	±6.71	56.4	39.6
	After exposure to hydrogen sulphide	7.97	0.464	0.9989	±5.20	49.4	39.2
	After exposure to ethane	8.37	0.467	0.9987	±5.60	51.0	39.3
TGS 2611-E00 B	Before gas exposure	9.68	0.495	0.9982	±6.86	52.0	50.3
	After exposure to acetylene	9.76	0.496	0.9982	±6.99	52.2	50.3
	After exposure to hydrogen sulphide	7.92	0.475	0.9988	±5.58	46.5	49.5
	After exposure to ethane	8.31	0.479	0.9986	±5.90	48.1	49.6

ethane, with the sensors taking some time to adjust to a new stable state. The same conclusions can be made for acetylene exposure, with no significant change observed for Logger A testing following acetylene exposure (which was the first exposed gas), yet a small change was observed for Logger B (with acetylene exposure conducted after hydrogen sulphide exposure). In any case, this test clearly shows that the gases present in the laboratory affected sensor behaviour. This is a key consideration during laboratory sensor testing, as well as for field deployment, where complex gas emissions may occur.

3.5. Water effect test

TGS gas characterisation using resistance ratios has been treated as independent of other environmental conditions (such as $[H_2O]$) in previous research, as discussed in Section 1. This assumes that a suitable R_r (derived with an identical

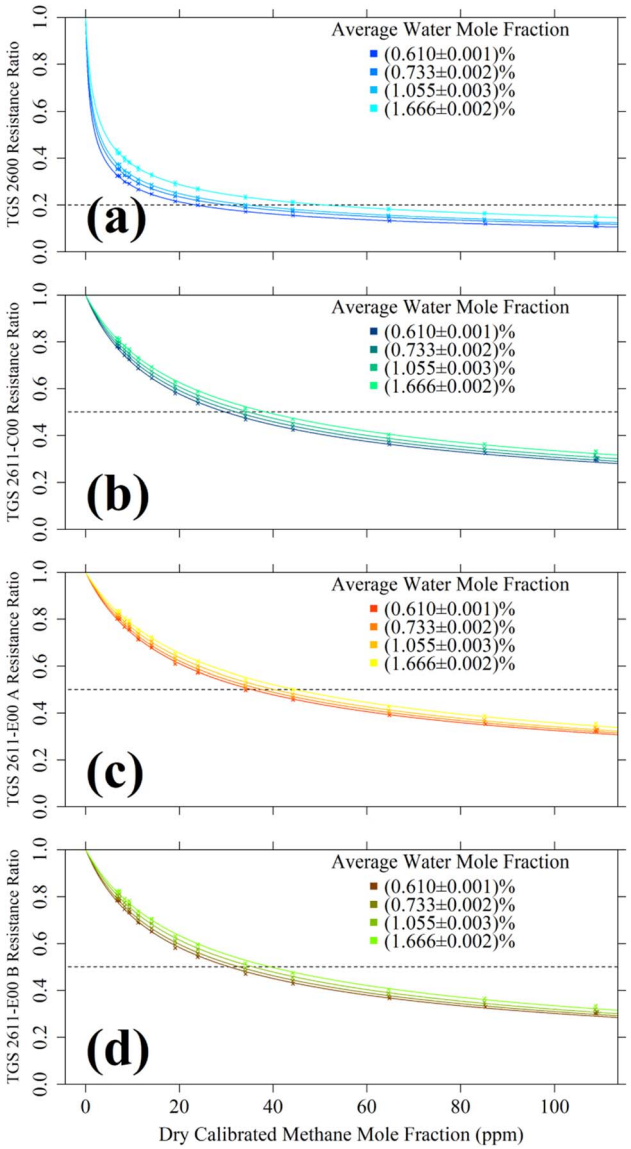

Fig. 10 $RR_{average}$ plotted as a function of $[CH_4]$ as coloured crosses for Test Type 3 Logger A SCS water effect tests at four different $[H_2O]$ levels for (a) TGS 2600, (b) TGS 2611-C00, (c) TGS 2611-E00 A and (d) TGS 2611-E00 B. The colour corresponding to each $[H_2O]$ level for each sensor is given in the legend, where each $[H_2O]$ level corresponds to average $[H_2O]$ when sampling raw $[CH_4]$ less than 5 ppm (average $[H_2O]$ for $[H_2O]$ level 1 excludes data from the end of the test, due to issues with the Picarro G2401 $[H_2O]$ measurement). Corresponding eqn (1) model fits are shown as coloured lines. A resistance ratio of 0.2 $\Omega\,\Omega^{-1}$ is indicated by a vertical dashed line in (a). A resistance ratio of 0.5 $\Omega\,\Omega^{-1}$ is indicated by a vertical dashed line in (b)–(d).

background gas composition) should incorporate any such environmental effects and cancel out within a resistance ratio. This is supported by tests conducted by Jørgensen *et al.*[52] who observed similar resistance ratio TGS fits at three different relative humidity settings. However, the precise effect of $[H_2O]$ changes on $[CH_4]$ derivation from resistance ratios has never been precisely tested, to our knowledge.

Therefore, Test Type 3 was conducted using Logger A at four different $[H_2O]$ levels ranging from 0.6% to 1.7% (see Section S3 in the SI), which was achieved by adjusting the dew-point setting of the dew-point generator (LI-610). The given $[H_2O]$ level corresponds to the average of all Picarro G2401 $[H_2O]$ measurements for periods sampling raw $[CH_4]$ less than 5 ppm during each test. At the lowest $[H_2O]$ level ($[H_2O]$ level 1), there were Picarro G2401 $[H_2O]$ spectral fitting issues towards the end of the test. Therefore, this data was discarded from the $[H_2O]$ average and a raw reported $[H_2O]$ second-order polynomial fit was derived without this final $[CH_4]_r$ sampling period. Gas characterisation resistance ratio curves for Test Type 3 water effect tests are presented in Fig. 10, with the gas characterisation coefficients, R^2 and RMSE of each model fit provided in Table 8, alongside the average R_r during periods used to derive R_r polynomial fits. Each of these four SCS water effect tests took place within 15 days.

Changes in TGS methane response were characterised using $\Delta[CH_4]_{0.5}$ for TGS 2611-C00, TGS 2611-E00 A and TGS 2611-E00 B, but using modelled methane mole fraction enhancement corresponding to a fixed resistance ratio of 0.2 $\Omega\,\Omega^{-1}$ ($\Delta[CH_4]_{0.2}$) for TGS 2600, due to its lower observed $RR_{average}$ range. These $\Delta[CH_4]_{0.5}$ and $\Delta[CH_4]_{0.2}$ values are given in Table 8 and are plotted against average $[H_2O]$ in Fig. 11. As noted in Section 2, $\Delta[CH_4]_{0.5}$ and $\Delta[CH_4]_{0.2}$ represent dry calibrated values. Fig. 11 shows a clear influence of $[H_2O]$ on resistance ratio fits, with $\Delta[CH_4]_{0.5}$ and $\Delta[CH_4]_{0.2}$ increasing with increasing $[H_2O]$. This effect occurs despite the expected cancelation of $[H_2O]$ effects through the use of resistance ratios. This effect is unlikely to be an artefact of the TGS stabilisation delay that occurs with changes in $[H_2O]$ (described in Shah *et al.*[51]), as the same dew-point setting was sampled at least 24 hours before the start of each test (as discussed in Section 2). Although linear fits are provided in Fig. 11 for illustration, a polynomial fit may be more apt. Yet, with only four data points, it is difficult to robustly characterise this effect without further testing. In any case, the magnitude of the change in $[CH_4]$ from this test is not directly transferrable to different conditions with a different background gas composition and from a different $[CH_4]_r$ level,[52,53,55] as discussed in Section 2. Resistance ratio gas characterisation conducted with an ambient background gas composition (instead of synthetic gases as in Test Type 3 SCS testing) and from a higher $[CH_4]_r$ level (as opposed to 0 ppm in this test) may result in a different effect on $\Delta[CH_4]$ (as evaluated in Section 4). Nevertheless, this test suggests that resistance ratio does not result in the total elimination of environmental effects, meaning that the importance of such effects on $\Delta[CH_4]$ estimation would have to be evaluated for the final sensor application depending on $[CH_4]_r$, the background gas composition and the expected $\Delta[CH_4]$ sampling range.

4. Sensor characterisation in ambient air analysis and results

Automatic SCA tests were conducted over a period of approximately 25 months, sampling an ambient background gas

Table 8 Gas characterisation coefficients from Test Type 3 Logger A SCS water effect tests with corresponding R^2 and RMSE values. $\Delta[CH_4]_{0.2}$ is given for TGS 2600 for each test. $\Delta[CH_4]_{0.5}$ is given for TGS 2611-C00, TGS 2611-E00 A and TGS 2611-E00 B for each test. The average R_r during periods used to derive R_r polynomial fits is given for each TGS

Sensor	Test status	m (ppm)	μ	R^2	RMSE (mΩ Ω^{-1})	$\Delta[CH_4]_{0.2}$ (ppm)	$\Delta[CH_4]_{0.5}$ (ppm)	R_r (kΩ)
TGS 2600	$[H_2O]$ level 1	0.469	0.409	0.9988	2.62	23.6	—	352
	$[H_2O]$ level 2	0.575	0.405	0.9985	3.16	30.1	—	313
	$[H_2O]$ level 3	0.664	0.405	0.9991	2.51	34.7	—	286
	$[H_2O]$ level 4	0.915	0.398	0.9977	4.64	51.1	—	217
TGS 2611-C00	$[H_2O]$ level 1	10.5	0.515	0.9990	5.46	—	29.8	63.1
	$[H_2O]$ level 2	11.5	0.519	0.9989	5.61	—	32.1	60.6
	$[H_2O]$ level 3	12.4	0.518	0.9989	5.72	—	34.8	56.1
	$[H_2O]$ level 4	13.4	0.511	0.9988	5.85	—	38.5	48.4
TGS 2611-E00 A	$[H_2O]$ level 1	11.9	0.500	0.9984	6.70	—	35.6	42.9
	$[H_2O]$ level 2	12.7	0.503	0.9984	6.69	—	37.7	41.5
	$[H_2O]$ level 3	14.3	0.516	0.9981	7.34	—	40.4	39.0
	$[H_2O]$ level 4	15.6	0.512	0.9983	6.87	—	44.8	34.2
TGS 2611-E00 B	$[H_2O]$ level 1	10.8	0.515	0.9981	7.38	—	30.7	56.2
	$[H_2O]$ level 2	11.8	0.522	0.9980	7.56	—	32.8	54.5
	$[H_2O]$ level 3	13.7	0.539	0.9975	8.58	—	35.8	51.4
	$[H_2O]$ level 4	15.0	0.537	0.9976	8.42	—	39.5	45.4

composition under different environmental conditions (including $[H_2O]$, [CO] and pressure) over time, to evaluate the effect of several variables on TGS sensor response for the four Logger A TGS units. For each of the 147 successful SCA tests, seven SCA testing variables were evaluated. Four of these SCA testing variables used an average of all measurements from the full duration of each test: SHT85 temperature, Picarro G2401 $[H_2O]$ (when raw $[CH_4]$ measurements were less than 5 ppm), Picarro G2401 [CO] and TGS V_s. Two of these SCA testing variables used an average of all measurements from periods used to derive R_r polynomial fits: $[CH_4]_r$ and modelled R_r for each TGS. The final SCA testing variable is time. The first six SCA testing variables are plotted as a function of time in Fig. 12. TGS response to these SCA testing variables was evaluated using two ambient testing evaluation values. $\Delta[CH_4]_{0.5}$ served as ambient testing evaluation values for the TGS 2611-C00, TGS 2611-E00 A and TGS 2611-E00 B, while $\Delta[CH_4]_{0.6}$ was used for the TGS 2600 due its overall higher $RR_{average}$ range during these tests. These ambient testing evaluation values ($\Delta[CH_4]_{0.5}$ and $\Delta[CH_4]_{0.6}$) are also plotted as a function of time in Fig. 12. The average and standard deviation of all 147 ambient testing evaluation values are provided in Table 9 for each TGS.

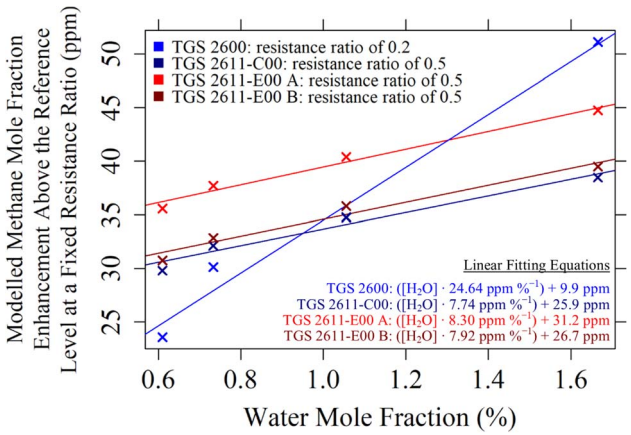

Fig. 11 Dry calibrated $\Delta[CH_4]_{0.2}$ for TGS 2600, $\Delta[CH_4]_{0.5}$ for TGS 2611-C00, $\Delta[CH_4]_{0.5}$ for TGS 2611-E00 A and $\Delta[CH_4]_{0.5}$ for TGS 2611-E00 B from Test Type 3 Logger A SCS water effect tests, all plotted as a function of average $[H_2O]$ (when sampling raw $[CH_4]$ less than 5 ppm; average $[H_2O]$ for $[H_2O]$ level 1 excludes data from the end of the test, due to issues with the Picarro G2401 $[H_2O]$ measurement) as coloured crosses (see legend in the top left-hand corner). Coloured lines representing linear fits are also given for each sensor (see bottom right-hand corner for linear fitting equations). $\Delta[CH_4]_{0.2}$ for TGS 2600 at (1.055 ± 0.003)% $[H_2O]$ is difficult to distinguish due to its proximity to $\Delta[CH_4]_{0.5}$ for TGS 2611-C00 at the same $[H_2O]$ level.

Fig. 12 shows consistently strong methane sensitivity for the full duration of testing through ambient testing evaluation values. However, there are variations in these ambient testing evaluation values between different tests. For example, TGS 2611-C00 has a $\Delta[CH_4]_{0.5}$ standard deviation variability of ±8 ppm. The cause of this variation was investigated by evaluating the correlation between ambient testing evaluation values and each SCA testing variable. Linear fits are plotted between ambient testing evaluation values and each SCA testing variable in Fig. 13, with corresponding Pearson correlation coefficient (r) values for each linear fit provided in Fig. 14 for the full SCA testing dataset. Fig. 14 correlation values show that time is an important factor governing TGS response to $[CH_4]$ enhancements.

However, Test Type 2 SCS temporal evolution tests presented in Section 3 show that Logger A TGS behaviour did not significantly change between 21 November 2023 and 11 September 2024, based on $\Delta[CH_4]_{0.8}$ results presented in Table 3. Therefore, it can be assumed that all SCA tests conducted in this time window were unaffected by inherent changes in TGS behaviour. In total, 60 successful SCA tests were conducted between Logger A Test Type 2 SCS temporal evolution tests on 21 November 2023 and 11 September 2024. Additional linear plots were

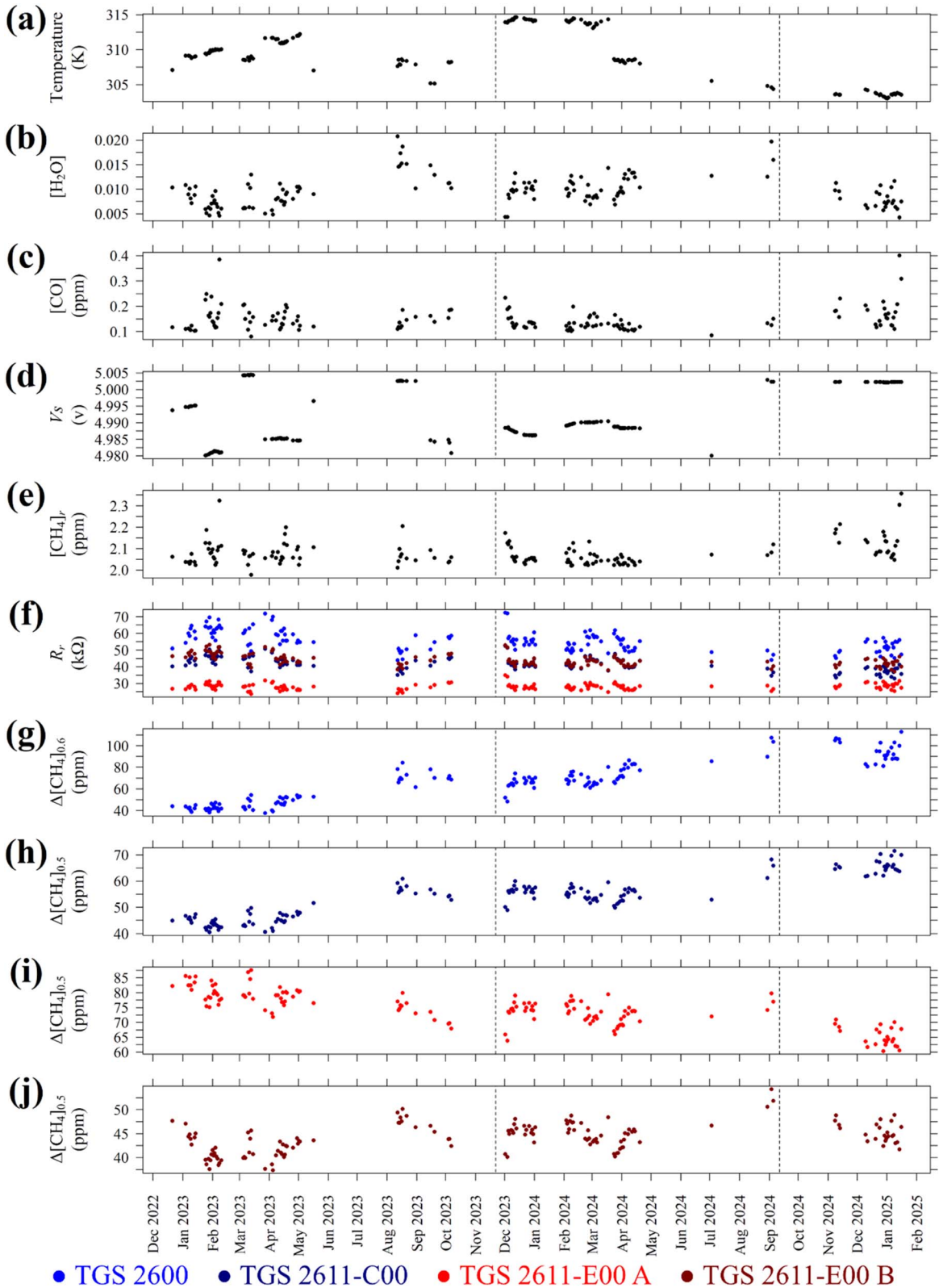

Fig. 12 The average (a) SHT85 temperature, (b) Picarro G2401 [H_2O] (at raw wet [CH_4] of less than 5 ppm), (c) Picarro G2401 [CO], (d) TGS V_s, (e) $[CH_4]_r$ and (f) R_r for each Logger A SCA test, with corresponding derived (g) TGS 2600 $\Delta[CH_4]_{0.6}$, (h) TGS 2611-C00 $\Delta[CH_4]_{0.5}$, (i) TGS 2611-E00 A $\Delta[CH_4]_{0.5}$ and (j) TGS 2611-E00 B $\Delta[CH_4]_{0.5}$. All averages are derived from the full duration of each test, expect for $[CH_4]_r$ and R_r averages, which are derived from periods used to derive R_r polynomial fits. Data corresponding to each TGS is shown as coloured dots (see legend). The time at which Test Type 2 Logger A SCS temporal evolution tests were conducted in November 2023 and September 2024 are shown as dashed vertical lines.

Table 9 Average and standard deviation of derived ambient testing evaluation values for each Logger A TGS from SCA tests. Values are given for the full dataset, as well as for the reduced dataset, corresponding to data points collected between Test Type 2 Logger A SCS temporal evolution tests in November 2023 and September 2024

Dataset	Number of data points	TGS 2600 $\Delta[CH_4]_{0.6}$ (ppm)	TGS 2611-C00 $\Delta[CH_4]_{0.5}$ (ppm)	TGS 2611-E00 A $\Delta[CH_4]_{0.5}$ (ppm)	TGS 2611-E00 B $\Delta[CH_4]_{0.5}$ (ppm)
Full	147	66 ± 19	54 ± 8	74 ± 6	44 ± 3
Reduced	60	71 ± 10	56 ± 3	73 ± 3	45 ± 3

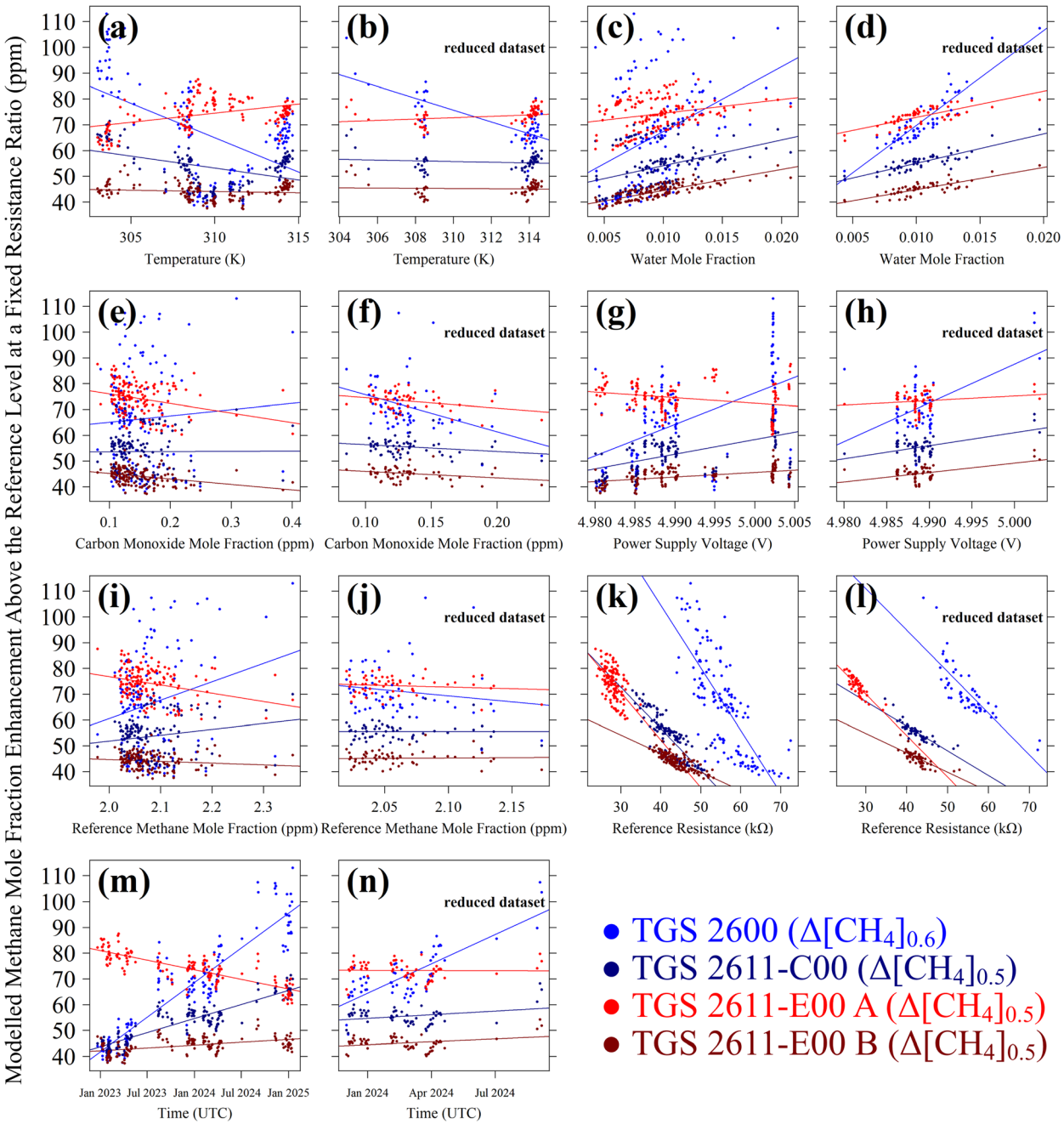

Fig. 13 Ambient testing evaluation values for each TGS from Logger A SCA tests plotted as coloured dots (see legend) against average (a) SHT85 temperature for the full dataset. (b) SHT85 temperature for the reduced dataset, (c) Picarro G2401 [H_2O] (at raw wet [CH_4] of less than 5 ppm) for the full dataset, (d) Picarro G2401 [H_2O] (at raw wet [CH_4] of less than 5 ppm) for the reduced dataset, (e) Picarro G2401 [CO] for the full dataset, (f) Picarro G2401 [CO] for the reduced dataset, (g) TGS V_s for the full dataset, (h) TGS V_s for the reduced dataset, (i) $[CH_4]_r$ for the full dataset, (j) $[CH_4]_r$ for the reduced dataset, (k) R_r for the full dataset, (l) R_r for the reduced dataset, (m) time for the full dataset and (n) time for the reduced dataset. All averages are derived from the full duration of each test, except for $[CH_4]_r$ and R_r averages, which are derived from periods used to derive R_r polynomial fits. The reduced dataset corresponds to any data points between Test Type 2 Logger A SCS temporal evolution tests in November 2023 and September 2024. R_r averages are unique for each TGS.

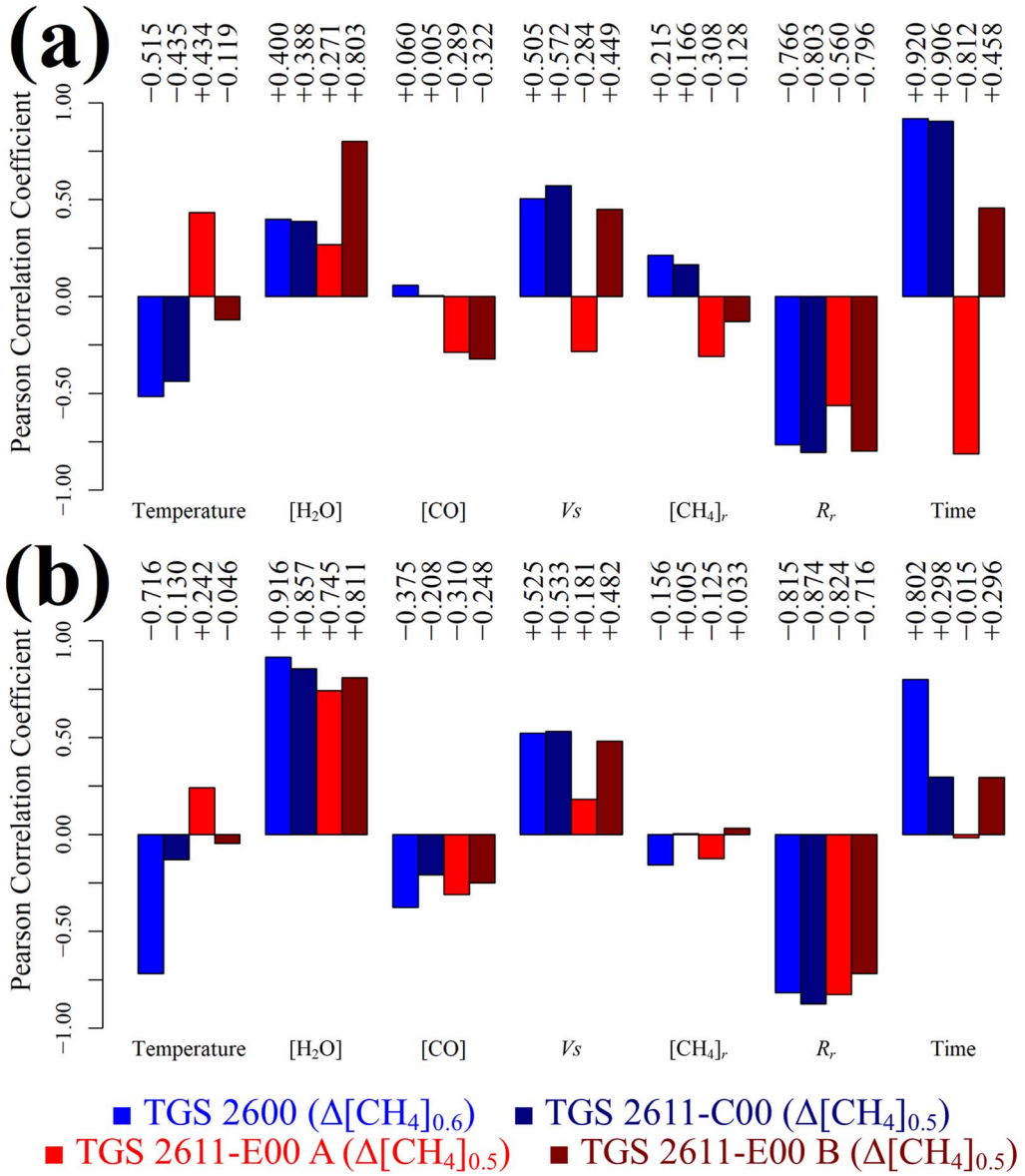

Fig. 14 r between ambient testing evaluation values for each TGS and each SCA testing variable from Logger A SCA tests, plotted as coloured bars (see legend) for (a) the full dataset and (b) the reduced dataset. The reduced dataset corresponds to any sampling data points between Test Type 2 Logger A SCS temporal evolution tests conducted in November 2023 and September 2024. R_r averages are unique for each TGS.

produced for this reduced dataset of 60 data points in Fig. 13, with corresponding r values given in Fig. 14. This shows a weaker time influence for this subset of the full dataset, which can also be observed from visual inspection of Fig. 12, where ambient testing evaluation values are more stable in the reduced time window (indicated by vertical dashed lines). The lower standard deviation variability in ambient testing evaluation values for this reduced dataset of 60 data points is provided in Table 9 for each Logger A TGS. For example, $\Delta[CH_4]_{0.5}$ variability for TGS 2611-C00 declines by 57% for the reduced dataset.

Although the influence of time declines for ambient testing evaluation values for each sensor for the reduced dataset (compared to the full dataset), it still remains a significant factor for TGS 2611-C00 (reduced r of +0.30 *versus* full r of +0.91) and TGS 2611-E00 B (reduced r of +0.30 *versus* full r of +0.46), with it remaining particularly strong for TGS 2600 (reduced r of +0.80 *versus* full r of +0.92). Yet this time correlation is not likely due to persistent changes in TGS behaviour, as discussed above, based on results from Logger A SCS temporal evolution tests at the start and end of this reduced sampling window. Furthermore, a consistently strong TGS 2600 $\Delta[CH_4]_{0.6}$ correlation with time for both the full and the reduced datasets may also suggest that this time correlation is unrelated to persistent changes in TGS behaviour, with relatively minor variation between any of the three Test Type 2 SCS temporal evolution tests for this specific sensor compared to the other three TGSs, which changed significantly between July 2023 and November 2023.

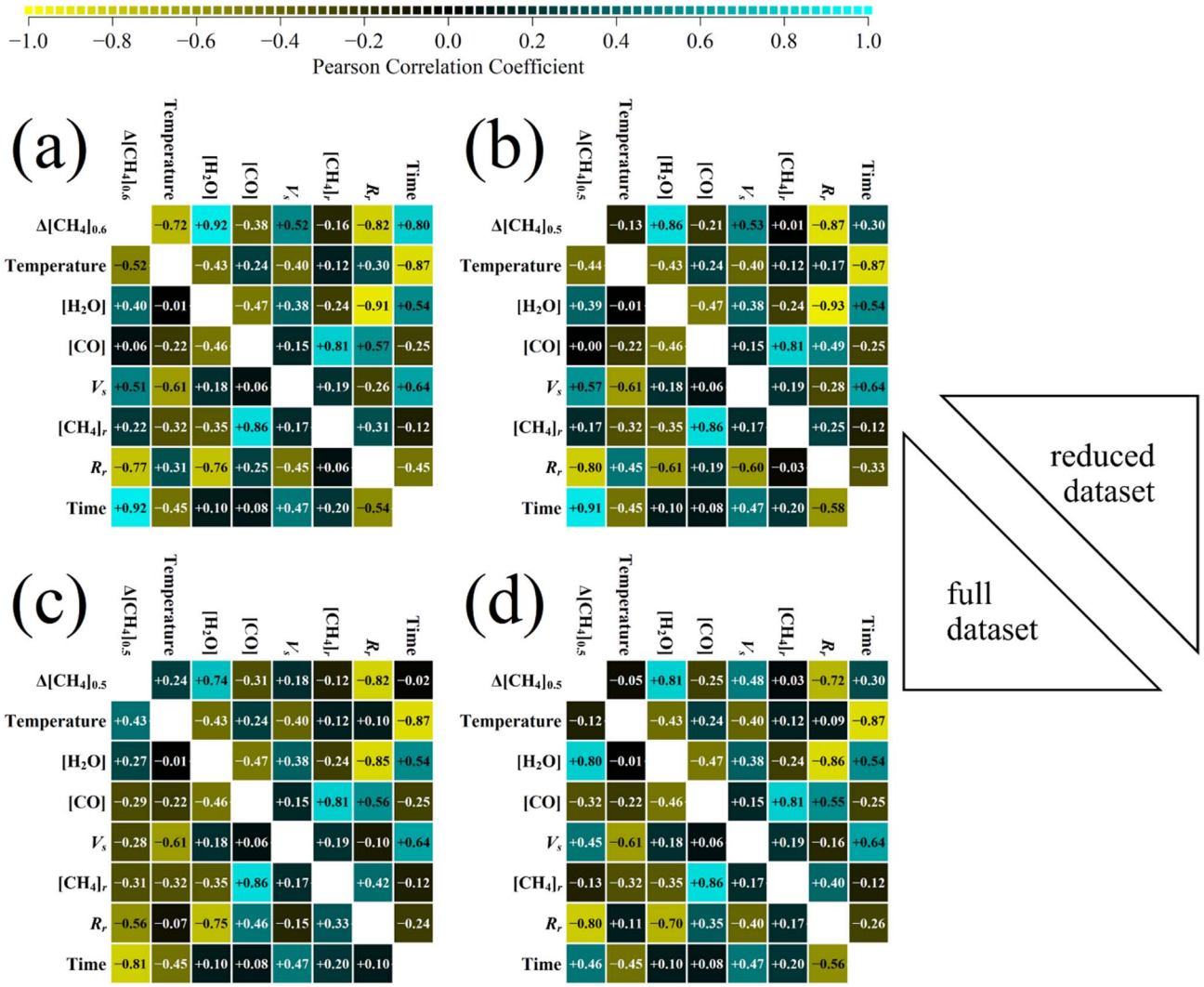

Fig. 15 r from Logger A SCA tests plotted as coloured squares between ambient testing evaluation values for each TGS and each SCA testing variable for (a) TGS 2600, (b) TGS 2611-C00, (c) TGS 2611-E00 A and (d) TGS 2611-E00 B. Correlation values for the full dataset are shown in the bottom-left-hand corner of each plot and correlation values for the reduced dataset (any sampling data points between Test Type 2 Logger A SCS temporal evolution tests conducted in November 2023 and September 2024) are shown in the top-right-hand corner of each plot. Back squares represent no correlation, yellow squares represent a negative correlation, and cyan squares represent a positive correlation (see colour scale). R_r averages are unique for each TGS.

Thus, the residual correlation of ambient testing evaluation values with time for the reduced dataset is probably due to the correlation between other SCA testing variables with time. This was investigated by producing a correlation matrix between each SCA testing variable and the ambient testing evaluation value for each TGS in Fig. 15, with r values for the full dataset given in the bottom-left-hand corner and r values for the reduced dataset given in the top-right-hand corner of each plot.

Fig. 15 values show that $[H_2O]$ is moderately correlated with time for the reduced dataset (r of +0.54), which may therefore explain why TGS 2600 $\Delta[CH_4]_{0.6}$ values are correlated with time for the same reduced dataset. This therefore confirms the observations from the SCS water effect tests, which show methane gas characterisation curves to be dependent on $[H_2O]$. All ambient testing evaluation values show some correlation with $[H_2O]$ for the full dataset, but these effects are amplified for the reduced dataset (see stronger correlation between ambient testing evaluation values and $[H_2O]$ in Fig. 14). This suggests that during a period of no presumed major long-term change in sensor behaviour, $[H_2O]$ is the key driver of sensor response to $\Delta[CH_4]$. Yet during the full sampling period (when correlation between $[H_2O]$ and time is far weaker, with a r of +0.10), time is strongly correlated with ambient testing evaluation values. Thus, rather than $[H_2O]$, long-term temporal changes in TGS methane sensitivity for the full dataset may be largely driven by sudden discrete incidents, such as incidents of exposure to certain atmospheric species, as presented in SCS gas exposure tests in Section 3.

Both the full and reduced datasets show a strong general correlation between R_r and ambient testing evaluation values

(see Fig. 14), which appears to be the key driver of sensor response. Hence, $[H_2O]$ also has a strong correlation with R_r (r of less than -0.8) for all four sensors in the reduced dataset, as observed elsewhere.[31] However, $[CH_4]_r$ does not exhibit a strong correlation with R_r (r of less than +0.5 for all sensors for both the full and reduced datasets). This is because $[CH_4]_r$ represents the pure ambient outdoor air level, which did not change significantly throughout the course of sampling, from the semi-rural location of our laboratory. As a consequence, Fig. 14 shows a weak correlation between $[CH_4]_r$ and ambient testing evaluation values. This confirms that the $\Delta[CH_4]$ above a small $[CH_4]_r$ range (close to 2 ppm) can successfully be used in this analysis to characterise the effect of other variables on TGS behaviour. $[CH_4]_r$ is not strongly correlated with any other SCA testing variable in Fig. 15 except [CO] (r of +0.86 for the full dataset and +0.81 for the reduced dataset), with [CO] also weakly correlated with ambient testing evaluation values. Although the average [CO] range spanned between 0.08 ppm and 0.41 ppm for all SCA tests (which is not small), only a weak correlation between [CO] and ambient testing evaluation values is observed due to the dominant effect of methane on TGS response compared to carbon monoxide, considering $[CH_4]_r$ and $\Delta[CH_4]$ levels. In more complex environments close to carbon monoxide emissions, this may become more significant, especially due to TGS interdependence effects between methane and carbon monoxide.[55]

Temperature appears to show some correlation with ambient testing evaluation values, especially with TGS 2600 $\Delta[CH_4]_{0.6}$ for the reduced dataset, with a r of -0.72. Previous research has also shown an influence of temperature on resistance ratio $[CH_4]$ fitting for large temperature ranges.[24] However, Fig. 15 shows that the correlation between ambient testing evaluation values and temperature in this study is most probably due to a strong r of -0.87 between temperature and time for the reduced dataset, which is only -0.45 for the full dataset. Previous work has shown temperature to have a minimal effect on resistance measurements at ambient baseline $[CH_4]$ levels.[38,51]

Finally, V_s is included in this analysis as it may be influenced by the hardware configuration, with the power supply potentially being affected by changes in wiring or power supply circuitry. Although power supply can slightly affect the TGS resistance ratio response,[51] it is not expected to be a key factor across the small 24 mV V_s range presented in Fig. 12. The values in Fig. 14 may suggest some moderate correlation between V_s and ambient testing evaluation values. However, visual inspection of Fig. 12 shows that while V_s appears to be moderately correlated with ambient testing evaluation values for certain periods, V_s does not appear to follow sensor response for the first part of the dataset (before November 2023). Therefore, this apparent correlation is likely due to other effects that vary with time (see Fig. 15), with a moderate correlation between V_s and time (r of +0.47 for the full dataset and +0.64 for the reduced dataset). Furthermore, V_s was almost constant for most of the reduced dataset, with only a few datapoints diverging from the average V_s level, which is the possible cause of the apparent moderate V_s correlation with ambient testing evaluation values for the reduced dataset. We therefore conclude that it is unlikely that the small V_s changes during testing influenced TGS methane response in this resistance ratio approach, with $[H_2O]$ instead being a key factor. Perhaps this can be the subject of future investigations with greater V_s variability under controlled environmental conditions.

Thus, to summarise this SCA testing work, reducing the dataset to a period assumed to contain no major sensor changes (based on similar results from Logger A Test Type 2 SCS temporal evolution tests) reveals $[H_2O]$ to be the dominant cause of variability in estimating $[CH_4]$ enhancements above $[CH_4]_r$ at a fixed resistance ratio level. Conversely, the correlation between time and ambient testing evaluation values is weaker for the reduced dataset compared to the full dataset, with much of this correlation likely due to $[H_2O]$ cross-correlation effects. This supports the conclusions of SCS temporal evolution tests that general ageing is not likely an issue with TGS methane sensitivity. However, persistent long-term sensor changes may instead be responsible for the stronger correlation of ambient testing evaluation values with time observed for the full dataset, where extreme or prolonged exposure to certain atmospheric species may have influenced overall TGS behaviour.

5. Discussion

This work set out to understand changes in TGS response to $[CH_4]$, as TGS sampling may be used as a low-cost solution to provide *in situ* $[CH_4]$ measurements downwind of facility-scale methane emission sources during prolonged autonomous field deployment. Two categories of tests were conducted to evaluate TGS methane sensitivity. SCS tests were conducted under controlled conditions, each with a stable $[H_2O]$ level (see $[H_2O]$ standard deviation values provided in Section S3 in the SI for each SCS test), where gases with a synthetic background gas composition were blended to various $\Delta[CH_4]$ levels. Meanwhile, SCA tests were conducted by adding a small amount of gas with a high $[CH_4]$ to an ambient outdoor air gas stream to obtain various $\Delta[CH_4]$ levels. In both tests, changes in methane sensitivity were evaluated using resistance ratios (with respect to R_r, representative of sampling at $[CH_4]_r$) to calculate changes in modelled $\Delta[CH_4]$ at a fixed specific resistance ratio level. A unique R_r polynomial model was derived for each test from measurements made during $[CH_4]_r$ sampling periods. Modelling R_r from $[CH_4]_r$ sampling allowed for independent and precise analysis of TGS methane response for each test, without convolving issues otherwise arising due to modelling R_r from environmental variables and time.

SCS temporal evolution tests revealed no major change in TGS methane response over a period of at least 9 months between November 2023 and September 2024 (see $\Delta[CH_4]_{0.5}$ values in Table 2 and $\Delta[CH_4]_{0.8}$ values in Table 3), with all of these tests being conducted under similar environmental conditions (see Section S3 in the SI for details). This suggests that natural drift through ageing is not a major factor determining TGS methane response when using resistance ratios. This implies that the same eqn (1) coefficients can be assumed

to be valid for the full duration of this time interval. Yet, a key change in sensor behaviour was observed between SCS temporal evolution tests conducted in July 2023 and November 2023 for these same sensors (see $\Delta[CH_4]_{0.8}$ values in Table 3). This suggests that rather than TGS ageing, the sensors were subject to a sudden behavioural change.

Further SCS testing investigated the cause of sudden changes in the TGS resistance ratio response. Dry exposure and power loss do not stand as likely candidates (see $\Delta[CH_4]_{0.6}$ values in Tables 4 and 5, respectively), although only one TGS was tested, so further analysis may be required to confirm this in future work. Instead, exposure to certain gases was found to cause abrupt changes in TGS response to $[CH_4]$, for all five sensors tested in this work. Of the three gases tested, hydrogen sulphide was found to have a clear and profound influence on TGS behaviour during SCS gas exposure tests. Elsewhere, Buturini and Fonollosa[38] also found high levels of hydrogen sulphide exposure to cause permanent TGS damage due to its corrosive nature.[56] This emphasises the importance of avoiding excessive or prolonged exposure to certain atmospheric species during methane gas characterisation testing, during final sensor application (to derive unknown mole fractions) and during the interval between these periods, although it is difficult to know which other species (due to their corrosive nature or otherwise) may affect the TGS and at which levels. A permanently installed supplementary protective TGS filter may help to avoid such issues.[46]

The results from SCA tests support the conclusions of SCS tests. For example, Test Type 2 SCS temporal evolution tests showed that each Logger A TGS had a similar methane response between November 2023 and September 2024 (see Table 3). This is consistent with the weaker $\Delta[CH_4]_{0.5}$ or $\Delta[CH_4]_{0.6}$ correlation with time for SCA tests when limited to this time range, compared to the full dataset. Yet, although correlation with time weakens, it does not diminish entirely, especially with a r of +0.80 between time and TGS 2600 $\Delta[CH_4]_{0.6}$ for the reduced dataset. This is most likely due to the effect of other environmental variables affecting methane response, which were themselves correlated with time, especially $[H_2O]$.

Use of a resistance ratio approach has previously been thought to eliminate the effect of environmental factors.[53] Yet both the SCS water effect tests and the SCA tests (for the reduced dataset) suggest the existence of a $[H_2O]$ effect on TGS methane response, when using resistance ratios. This $[H_2O]$ effect may be due to the strong direct $[H_2O]$ effect on TGS resistance in the absence of $[CH_4]$ enhancements,[15,28,30,31,39,46–48,50,51] leaving a resistance ratio unable to fully incorporate $[H_2O]$ effects. For example, Fig. 11 shows that a fixed measured resistance ratio can yield different resulting $\Delta[CH_4]$ estimates depending on $[H_2O]$. TGS 2611-C00 $\Delta[CH_4]_{0.5}$ is 29.8 ppm at a $[H_2O]$ of 0.61% but this increases to 38.5 ppm at a $[H_2O]$ of 1.67% for this specific test. A supplementary $[H_2O]$ correction may be formulated for inclusion as an additional eqn (1) term. Yet, an 8.7 ppm $\Delta[CH_4]_{0.5}$ increase over a 1.1% $[H_2O]$ range (for this specific SCS example) may not be so important, depending on the final sensor application. Furthermore, Test Type 3 SCS water effect tests were conducted from a $[CH_4]_r$ of 0 ppm, which can enhance changes in resistance ratio fits (as larger changes in resistance ratio for a small $\Delta[CH_4]$ may occur at lower $[CH_4]_r$ levels). This $[H_2O]$ effect may reduce depending on $[CH_4]_r$ and the background gas composition. For example, $\Delta[CH_4]_{0.5}$ had a standard deviation variability of only $\pm$3 ppm for TGS 2611-C00 from SCA tests for the reduced dataset, with this variability principally attributed to $[H_2O]$. As general guidance, if assuming resistance ratio gas response to be independent of $[H_2O]$ in future work, it is recommended to conduct methane gas characterisation at a $[H_2O]$ level typical of $[H_2O]$ expected during the final sensor application.

The required $\Delta[CH_4]$ measurement range above $[CH_4]_r$ is an important consideration when selecting a suitable sensor for the required application. It is interesting to note that $\Delta[CH_4]_{0.8}$ from Test Type 2 SCS temporal evolution tests increased significantly from July 2023 to November 2023 for each Logger A TGS except the TGS 2600 (see Table 3). This translates to an increase in $\Delta[CH_4]$ required to obtain the same 20% R_r decrease (*i.e.* a resistance ratio of 0.8). This change may be advantageous if greater sensitivity is required in a higher $\Delta[CH_4]$ range but is less suitable for lower $\Delta[CH_4]$ levels. Meanwhile, the opposite was observed during Test Type 3 SCS gas exposure tests for Logger A (see Table 7). Following hydrogen sulphide exposure, $\Delta[CH_4]_{0.4}$ decreased for each Logger A TGS and the $[CH_4]$ resistance ratio curves became steeper (see Fig. 9). This means that a lower $\Delta[CH_4]$ would be required to reach the same 60% R_r decrease (*i.e.* a resistance ratio of 0.4) after hydrogen sulphide exposure. This change is conducive to measuring smaller $\Delta[CH_4]$ levels. The different direction for these two tests may be due to the different $[CH_4]_r$ in Test Type 2 (0.5 ppm) compared to Test Type 3 (0 ppm). In any case, this result does not show conclusive TGS improvement or degradation in one direction or the other. It can only be concluded that the sensor becomes better optimised to measure in a certain $\Delta[CH_4]$ range, depending on the circumstances of sampling, including $[CH_4]_r$.

Considering the three different TGS types tested in this work, each exhibits clear methane sensitivity, with the TGS 2600 showing the largest resistance ratio change at low $\Delta[CH_4]$ levels, whereas the TGS 2611-C00 and the TGS 2611-E00 responded more gradually to $\Delta[CH_4]$. But with only a solitary TGS 2600 and TGS 2611-C00 inside Logger A, it is difficult to make general assertions on the transferability of these outcomes to other sensors of the same types. It is interesting to note that TGS 2611-E00 A and TGS 2611-E00 B reacted differently throughout this work. This may be associated with the different production batches from which these two sensors were sourced or the different conditions to which these two sensors were exposed over their lifetimes, which may be related to their age difference. It is also noteworthy that TGS 2600, TGS 2611-C00 and TGS 2611-E00 B all showed a clear methane response throughout testing despite the fact that they were at least three years old at the start of this work. This reiterates the insignificance of ageing concerning TGS sampling capability over this period, for the $[CH_4]$ ranges studied in this work.

The TGS 2600 methane sensitivity observed in this work is consistent with numerous previous studies.[34,35,44,45,47,48] The TGS 2600 may be advantageous due to its fast measurement

response and the large resistance ratio change in response to a small $\Delta[CH_4]$, compared to the other TGS types tested here. Yet Furuta *et al.*[30] observed a weak correlation between $[CH_4]$ and TGS 2600 resistance, although they sampled across a lower $[CH_4]$ range under a variety of environmental sampling conditions and did not use the resistance ratio approach demonstrated here. However, a subsequent study by Furuta *et al.*[31] using dynamic R_r to derive $[CH_4]$ from resistance ratios also found poor TGS 2600 methane sensitivity. While we observed a strong TGS 2600 methane response in this work, this may be because a unique R_r polynomial fit was derived for each test, rather than deriving a R_r model from a limited set of environmental measurements, as in this previous study.[31] A polynomial R_r model eliminates the effect of unknown environmental factors for precise laboratory characterisation testing, as demonstrated in this work. But this is not a practical approach for autonomous field sampling.

The change in methane sensitivity observed in this work may be related to changes in R_r. A previous study by Shah *et al.*[51] found a significant R_r change between two time periods. R_r for the full SCA testing dataset is moderately correlated with time for TGS 2600, TGS 2611-C00 and TGS 2611-E00 B with r values of −0.54, −0.58 and −0.56, respectively. Similarly, R_r for the full dataset is strongly correlated with $\Delta[CH_4]_{0.6}$ for TGS 2600, $\Delta[CH_4]_{0.5}$ for TGS 2611-C00 and $\Delta[CH_4]_{0.5}$ for TGS 2611-E00 B with r values of −0.77, −0.80 and −0.80, respectively. This suggests that extreme or prolonged exposure to certain atmospheric species, which cause long-term sensitivity changes, may also be linked to changes in R_r over time. This is supported by Furuta *et al.*,[31] who suggest that rather than natural drift, R_r changes abruptly. Average R_r values from SCS tests may also support this view. For example, TGS 2600 average R_r decreased from 313 kΩ before hydrogen sulphide exposure to 229 kΩ after hydrogen sulphide exposure for Test Type 3 SCS gas exposure tests (see Table 7). However, not all of the sensors behaved in such a conclusive way, for example TGS 2611-E00 A average R_r decreased slightly from 39.6 kΩ before hydrogen sulphide exposure to 39.2 kΩ after hydrogen sulphide exposure for Test Type 3 SCS gas exposure tests (see Table 7), which is a far less significant than the corresponding large $\Delta[CH_4]_{0.4}$ decrease for the same test. Sudden R_r changes, due to potential factors such as exposure to certain species, may explain why it is difficult to model R_r over time solely from $[H_2O]$ and temperature for prolonged field sampling,[31,53] which are otherwise the key drivers in R_r variability. Further work is required to investigate the link between R_r and methane sensitivity.

To summarise, we show that natural ageing is unlikely to affect TGS methane response, as opposed to exposure to certain atmospheric species. Furthermore, we show $[H_2O]$ to have a clear influence on the $[CH_4]$ resistance ratio response. Yet despite the influence of environmental conditions highlighted in this work, resistance ratio $[CH_4]$ fits using fixed coefficients (independent of environmental effects) have successfully been demonstrated in the past. Jørgensen *et al.*[52] derived TGS 2611-E00 $[CH_4]$ from a resistance ratio power fit using fixed fitting coefficients, where stable environmental conditions allowed a fixed R_r to be used. Up to approximately 90 ppm $[CH_4]$ was measured with a RMSE of ±1.69 ppm compared to a high precision reference instrument, although the same ambient outdoor field sampling data were used to produce the resistance ratio fit.[52] Furuta *et al.*[31] made great progress in using resistance ratios to derive TGS 2611-E00 $[CH_4]$ with a piecewise R_r model based on temperature, $[H_2O]$, a time-dependent factor and TGS 2600 resistance (which they assumed to be methane insensitive), where $\Delta[CH_4]$ was limited to approximately 8 ppm. They used a linear $[CH_4]$ resistance ratio model, resulting in a $[CH_4]$ RMSE of ±0.65 ppm compared to $[CH_4]$ from a reference instrument when sampling ambient laboratory air.[31] However, this study also did not test autonomous sensor deployment, instead using the full dataset to model $[CH_4]$ as a function of resistance ratio.[31] Shah *et al.*[53] demonstrated TGS 2611-C00 $[CH_4]$ derivation at a landfill site, with a $[CH_4]$ RMSE of less than ±1 ppm compared to a high precision reference instrument. Laboratory-derived eqn (1) coefficients obtained in an ambient background gas composition (but erroneously derived in the absence of carbon monoxide) were applied to ambient outdoor field sampling to derive autonomous $[CH_4]$, where R_r was modelled using temperature, $[H_2O]$ and a time-dependent factor.[53] Although $\Delta[CH_4]$ reached up to 30 ppm, sampling was mostly close to $[CH_4]_r$ (*i.e.* $\Delta[CH_4]$ close to zero), demonstrating this to be a suitable approach to derive $[CH_4]$ with a sufficient accuracy when mostly sampling at low $[CH_4]$ levels,[53] despite potential changes in the nature of TGS methane response at different $[H_2O]$ levels.

These previous studies using a resistance ratio (assumed to be independent of environmental conditions) did not include an ageing factor to account for drift when deriving $[CH_4]$ from resistance ratio in field sampling.[31,52,53] The results of this work prove this to be a sensible approach, as time is unlikely to be a major intrinsic factor governing changes in resistance ratio characterisation as a function of $[CH_4]$, with $[H_2O]$ typically a minor factor in resistance ratio $[CH_4]$ characterisation conducted with an ambient background gas composition, considering overall accuracy requirements. However, caution must be taken to avoid excessive exposure to certain atmospheric species to ensure for consistent and stable resistance ratio $[CH_4]$ fits in future work. The issue of sudden changes in TGS behaviour may be overcome in future studies by conducting regular TGS calibrations throughout the year, across a $\Delta[CH_4]$ range expected in the final application. Sudden changes in $[CH_4]$ characterisation fits (as a function of resistance ratio) would be indicative of changes in TGS behaviour (due to damaging atmospheric exposure or otherwise). This would allow the data between such events to be flagged for removal and for new $[CH_4]$ coefficients to be used for subsequent periods with stable TGS behaviour, with respect to resistance ratios.

6. Conclusion

An extensive multitude of tests were performed on various TGS models to characterise changes in methane sensitivity. Two TGS loggers were used: Logger A contains one TGS 2600, one TGS 2611-C00 and two TGS 2611-E00 units; Logger B contains a single TGS 2611-E00. In each test, $[CH_4]$ was raised from

a $[CH_4]_r$ level up to a maximum $\Delta[CH_4]$ in discrete steps. TGS resistance measurements at elevated $[CH_4]$ were compared to a R_r, which was derived in this work by applying a polynomial fit as a function of time to $[CH_4]_r$ sampling periods. The $RR_{average}$ between measured resistance and R_r at each elevated $[CH_4]$ level was used to produce a two-term power fit, as a function of $\Delta[CH_4]$. This fit allowed a $\Delta[CH_4]$ value to be derived at a fixed specific resistance ratio level, the change in which throughout different tests was used to evaluate changes in TGS methane response.

SCS testing was conducted under controlled conditions, sampling blends with a synthetic background gas composition, using Logger A and Logger B in three different test types. Meanwhile. 147 successful SCA tests were automatically conducted with Logger A, sampling ambient outdoor air to which small quantities of gas with a high $[CH_4]$ were added. The results from SCS tests suggest that natural sensor ageing is not a key factor concerning TGS methane response, with similar resistance ratio fits observed when conducted at least 9 months apart. This means that the same gas characterisation coefficients can be valid over a prolonged sampling period. SCA tests support this conclusion, with a weaker correlation between time and methane response observed in this time window for the same TGSs.

However, SCS tests showed that exposure to certain atmospheric species can cause a sudden change in TGS methane sensitivity. Hydrogen sulphide exposure resulted in a clear and abrupt change in resistance ratio methane response, with ethane and acetylene exposure unlikely to be important factors. Other species may also be responsible, which would need to be assessed in future work. Exposure to such atmospheric species needs to be avoided both in the final sensor application, as well as during laboratory testing, to ensure the long-term validity of resistance ratio gas characterisation coefficients. Yet SCS tests did not appear to show power loss and dry sampling to have an effect on sensor behaviour for one tested TGS.

SCS tests did, however, show that $[H_2O]$ can affect the nature of resistance ratio fits. Therefore, the effect of $[H_2O]$ does not cancel out entirely when calculating a resistance ratio. A $[H_2O]$ correlation with TGS methane sensitivity was also observed during SCA testing. This may explain why there was a residual correlation of time with methane response during the reduced SCA testing sampling window, assumed to contain no long-term change in sensor behaviour. The importance of the $[H_2O]$ effect on resistance ratio fits may depend on the specific TGS being used, $[CH_4]_r$ during gas characterisation, the background gas composition and the expected $\Delta[CH_4]$ range. In previous studies, this $[H_2O]$ effect has not been an issue, considering the required $[CH_4]$ accuracy in final TGS applications to derive unknown $[CH_4]$ from this low-cost sensor technology. Taking these precautions and considerations into account allows these sensors to be used to measure *in situ* $[CH_4]$ downwind of facility-scale methane emission sources and, hence, to help improve our understanding of the global methane budget.

Author contributions

AS wrote the initial draft of the manuscript, which was edited by GB and OL. AS conducted laboratory testing with support from OL, who secured laboratory resources. AS designed the TGS logging systems, devised the method and conducted data analysis. CR and PC secured funding for this work.

Conflicts of interest

There are no conflicts to declare.

Data availability

All SCS and SCS testing data are available to access on the Internet.[59]

The electronic supplementary information contains six sections: S1. Supplementary logger details; S2. Picarro G2401 data interpolation; S3. List of sensor characterisation in synthetic air tests; S4. Laboratory description of sensor characterisation in synthetic air tests; S5. Laboratory description of sensor characterisation in ambient air tests; S6. Quality control of sensor characterisation in ambient air tests. See DOI: **https://doi.org/10.1039/d5ea00046g**.

Acknowledgements

This work received funding from the Integrated Carbon Observation System National Network France and from SUEZ Air & Climate. This work also received contributions in kind from the Chaire Industrielle TRACE, which is co-funded by the Agence Nationale de la Recherche (ANR) French National Research Agency (grant number: ANR-17-CHIN-0004-01), SUEZ Air & Climate, TotalEnergies OneTech and Thales Alenia Space.

References

1 M. Saunois, A. R. Stavert, B. Poulter, P. Bousquet, J. G. Canadell, R. B. Jackson, P. A. Raymond, E. J. Dlugokencky, S. Houweling, P. K. Patra, P. Ciais, V. K. Arora, D. Bastviken, P. Bergamaschi, D. R. Blake, G. Brailsford, L. Bruhwiler, K. M. Carlson, M. Carrol, S. Castaldi, N. Chandra, C. Crevoisier, P. M. Crill, K. Covey, C. L. Curry, G. Etiope, C. Frankenberg, N. Gedney, M. I. Hegglin, L. Höglund-Isaksson, G. Hugelius, M. Ishizawa, A. Ito, G. Janssens-Maenhout, K. M. Jensen, F. Joos, T. Kleinen, P. B. Krummel, R. L. Langenfelds, G. G. Laruelle, L. Liu, T. Machida, S. Maksyutov, K. C. McDonald, J. McNorton, P. A. Miller, J. R. Melton, I. Morino, J. Müller, F. Murguia-Flores, V. Naik, Y. Niwa, S. Noce, S. O'Doherty, R. J. Parker, C. Peng, S. Peng, G. P. Peters, C. Prigent, R. Prinn, M. Ramonet, P. Regnier, W. J. Riley, J. A. Rosentreter, A. Segers, I. J. Simpson, H. Shi, S. J. Smith, L. P. Steele, B. F. Thornton, H. Tian, Y. Tohjima, F. N. Tubiello, A. Tsuruta, N. Viovy, A. Voulgarakis, T. S. Weber, M. van Weele, G. R. van der Werf, R. F. Weiss, D. Worthy, D. Wunch, Y. Yin,

Y. Yoshida, W. Zhang, Z. Zhang, Y. Zhao, B. Zheng, Q. Zhu, Q. Zhu and Q. Zhuang, *Earth Syst. Sci. Data*, 2022, **12**, 1561–1623, DOI: 10.5194/essd-12-1561-2020.

2 E. G. Nisbet, M. R. Manning, E. J. Dlugokencky, S. E. Michel, X. Lan, T. Röckmann, H. A. C. D. van der Gon, J. Schmitt, P. I. Palmer, M. N. Dyonisius, Y. Oh, R. Fisher, D. Lowry, J. France, J. W. C. White, G. Brailsford and T. Bromley, *Global Biogeochem. Cycles*, 2023, **37**, e2023GB007875, DOI: 10.1029/2023gb007875.

3 M. Saunois, A. Martinez, B. Poulter, Z. Zhang, P. Raymond, P. Regnier, J. G. Canadell, R. B. Jackson, P. K. Patra, P. Bousquet, P. Ciais, E. J. Dlugokencky, X. Lan, G. H. Allen, D. Bastviken, D. J. Beerling, D. A. Belikov, D. R. Blake, S. Castaldi, M. Crippa, B. R. Deemer, F. Dennison, G. Etiope, N. Gedney, L. Höglund-Isaksson, M. A. Holgerson, P. O. Hopcroft, G. Hugelius, A. Ito, A. K. Jain, R. Janardanan, M. S. Johnson, T. Kleinen, P. Krummel, R. Lauerwald, T. Li, X. Liu, K. C. McDonald, J. R. Melton, J. Mühle, J. Müller, F. Murguia-Flores, Y. Niwa, S. Noce, S. Pan, R. J. Parker, C. Peng, M. Ramonet, W. J. Riley, G. Rocher-Ros, J. A. Rosentreter, M. Sasakawa, A. Segers, S. J. Smith, E. H. Stanley, J. Thanwerdas, H. Tian, A. Tsuruta, F. N. Tubiello, T. S. Weber, G. van der Werf, D. E. Worthy, Y. Xi, Y. Yoshida, W. Zhang, B. Zheng, Q. Zhu, Q. Zhu and Q. Zhuang, *Earth Syst. Sci. Data*, 2025, **17**, 1873–1958, DOI: 10.5194/essd-17-1873-2025.

4 E. J Dlugokencky, E. G. Nisbet, R. Fisher and D. Lowry, *Philos. Trans. R. Soc., A*, 2011, **369**, 2058–2072, DOI: 10.1098/rsta.2010.0341.

5 T. A. Fox, T. E. Barchyn, D. Risk, A. P. Ravikumar and C. H. Hugenholtz, *Environ. Res. Lett.*, 2019, **14**, 053002, DOI: 10.1088/1748-9326/ab0cc3.

6 A. L. Ganesan, S. Schwietzke, B. Poulter, T. Arnold, X. Lan, M. Rigby, F. R. Vogel, G. R. van der Werf, G. Janssens-Maenhout, H. Boesch, S. Pandey, A. J. Manning, R. B. Jackson, E. G. Nisbet and M. R. Manning, *Global Biogeochem. Cycles*, 2019, **33**, 1475–1512, DOI: 10.1029/2018gb006065.

7 M. B. Erland, A. K. Thorpe and J. A. Gamon, *Environ. Sci. Technol.*, 2022, **56**, 16567–16581, DOI: 10.1021/acs.est.2c02136.

8 E. Nisbet and R. Weiss, *Science*, 2010, **328**, 1241–1243, DOI: 10.1126/science.1189936.

9 A. R. Stavert, M. Saunois, J. G. Canadell, B. Poulter, R. B. Jackson, P. Regnier, R. Lauerwald, P. A. Raymond, G. H. Allen, P. K. Patra, P. Bergamaschi, P. Bousquet, N. Chandra, P. Ciais, A. Gustafson, M. Ishizawa, A. Ito, T. Kleinen, S. Maksyutov, J. McNorton, J. R. Melton, J. Müller, Y. Niwa, S. Peng, W. J. Riley, A. Segers, H. Tian, A. Tsuruta, Y. Yin, Z. Zhang, B. Zheng and Q. Zhuang, *Glob. Change Biol.*, 2021, **28**, 182–200, DOI: 10.1111/gcb.15901.

10 M. R. Johnson, B. M. Conrad and D. R. Tyner, *Commun. Earth Environ.*, 2023, **4**, 139, DOI: 10.1038/s43247-023-00769-7.

11 J. Hodgkinson and R. P. Tatam, *Meas. Sci. Technol.*, 2013, **24**, 012004, DOI: 10.1088/0957-0233/24/1/012004.

12 J. T. Shaw, A. Shah, H. Yong and G. Allen, *Philos. Trans. R. Soc., A*, 2021, **379**, 20200450, DOI: 10.1098/rsta.2020.0450.

13 T. Hong, J. T. Culp, K. J. Kim, J. Devkota, C. Sun and P. R. Ohodnicki, *Trends Anal. Chem.*, 2020, **125**, 115820, DOI: 10.1016/j.trac.2020.115820.

14 X. Yang, E. Kuru, X. Zhang, S. Zhang, R. Wang, J. Ye, D. Yang, J. J. Klemeš and B. Wang, *J. Clean. Prod.*, 2023, **414**, 137693, DOI: 10.1016/j.jclepro.2023.137693.

15 J. Watson, K. Ikohura and G. S. V. Coles, *Meas. Sci. Technol.*, 1993, **4**, 711–719, DOI: 10.1088/0957-0233/4/7/001.

16 S. D. Choi and D. D. Lee, *Sens. Actuators, B*, 2001, **77**, 335–358, DOI: 10.1016/s0925-4005(01)00727-4.

17 J. Glöckler, C. Jaeschke, E. Tütüncü, V. Kokoric, Y. Kocaöz and B. Mizaikoff, *Anal. Bioanal. Chem.*, 2020, **412**, 4575–4584, DOI: 10.1007/s00216-020-02705-6.

18 D. Kohl, *Sensor. Actuator.*, 1989, **18**, 71–113, DOI: 10.1016/0250-6874(89)87026-x.

19 D. Kohl, *Sens. Actuators, B*, 1990, **1**, 158–165, DOI: 10.1016/0925-4005(90)80193-4.

20 U. Hoefer, J. Frank and M. Fleischer, *Sens. Actuators, B*, 2001, **78**, 6–11, DOI: 10.1016/s0925-4005(01)00784-5.

21 D. Kohl, *J. Phys. D: Appl. Phys.*, 2001, **34**, R125–R149, DOI: 10.1088/0022-3727/34/19/201.

22 N. Barsan, D. Koziej and U. Weimar, *Sens. Actuators, B*, 2007, **121**, 18–35, DOI: 10.1016/j.snb.2006.09.047.

23 H. Suto and G. Inoue, *J. Atmos. Ocean. Technol.*, 2010, **27**, 1175–1184, DOI: 10.1175/2010jtecha1400.1.

24 P. K. Clifford and D. T. Tuma, *Sensor. Actuator.*, 1983, **3**, 233–254, DOI: 10.1016/0250-6874(82)80026-7.

25 U. Weimer, K. D. Schierbaum, W. Göpel and R. Kowalkowski, *Sens. Actuators, B*, 1990, **1**, 93–96, DOI: 10.1016/0925-4005(90)80179-4.

26 P. Massok, M. Loesch and D. Bertrand, *Sens. Actuators, B*, 1995, **25**, 525–528, DOI: 10.1016/0925-4005(95)85113-5.

27 A. C. Romain and J. Nicolas, *Sens. Actuators, B*, 2010, **146**, 502–506, DOI: 10.1016/j.snb.2009.12.027.

28 M. van den Bossche, N. T. Rose and S. F. J. De Wekker, *Sens. Actuators, B*, 2017, **238**, 501–509, DOI: 10.1016/j.snb.2016.07.092.

29 E. M. Taguem, L. Mennicken and A. C. Romain, *Sens. Actuators, B*, 2021, **324**, 129590, DOI: 10.1016/j.snb.2021.129590.

30 D. Furuta, T. Sayahi, J. Li, B. Wilson, A. A. Presto and J. Li, *Atmos. Meas. Tech.*, 2022, **15**, 5117–5128, DOI: 10.5194/amt-15-5117-2022.

31 D. Furuta, B. Wilson, A. A. Presto and J. Li, *Atmos. Meas. Tech.*, 2024, **17**, 2103–2121, DOI: 10.5194/amt-17-2103-2024.

32 P. R. Dando, P. Jensen, S. C. M. O'Hara, S. J. Niven, R. Schmajohann, U. Schuster and L. J. Taylor, *Bull. Geol. Soc. Den.*, 1994, **41**, 65–79, DOI: 10.37570/bgsd-1995-41-07.

33 J. Orts, E. Llobert, X. Vilanova, J. Brezmes and X. Correig, *Sens. Actuators, B*, 1999, **60**, 106–117, DOI: 10.1016/s0925-4005(99)00257-9.

34 W. Eugster and G. W. Kling, *Atmos. Meas. Tech.*, 2012, **5**, 1925–1934, DOI: 10.5194/amt-5-1925-2012.

35 A. Collier-Oxandale, J. G. Casey, R. Piedrahita, J. Ortega, H. Halliday, J. Johnston and M. P. Hannigan, *Atmos. Meas. Tech.*, 2018, **11**, 3569–3594, DOI: **10.5194/amt-11-3569-2018**.
36 J. G. Casey, A. Collier-Oxandale and M. Hannigan, *Sens. Actuators, B*, 2019, **283**, 504–514, DOI: **10.1016/j.snb.2018.12.049**.
37 A. Collier-Oxandale, N. Wong, S. Navarro, J. Johnston and M. Hannigan, *Atmos. Environ.*, 2020, **233**, 117519, DOI: **10.1016/j.atmosenv.2020.117519**.
38 A. Butturini and J. Fonollosa, *Limnol. Oceanogr.*, 2022, **20**, 710–720, DOI: **10.1002/lom3.10515**.
39 Y. Cho, K. M. Smits, S. N. Riddick and D. J. Zimmerle, *Sens. Actuators, B*, 2022, **355**, 131276, DOI: **10.1016/j.snb.2021.131276**.
40 D. Bastviken, J. Nygren, J. Schenk, R. Parellada Massana and N. T. Duc, *Biogeosciences*, 2020, **17**, 3659–3667, DOI: **10.5194/bg-17-3659-2020**.
41 A. K. Sieczko, N. T. Duc, J. Schenk, G. Pajala, D. Rudberg, H. O. Sawakuchi and D. Bastviken, *Proc. Natl. Acad. Sci. U. S. A.*, 2020, **117**, 21488–21494, DOI: **10.1073/pnas.2006024117**.
42 S. N. Riddick, R. Ancona, F. Cheptonui, C. S. Bell, A. Duggan, K. E. Bennett and D. J. Zimmerle, *Elem. Sci. Anth.*, 2022, **10**, 00021, DOI: **10.1525/elementa.2022.00021**.
43 R. Rivera-Martinez, P. Kumar, O. Laurent, G. Broquet, C. Caldow, F. Cropley, D. Santaren, A. Shah, C. Mallet, M. Ramonet, L. Rivier, C. Juery, O. Duclaux, C. Bouchet, E. Allegrini, H. Utard and P. Ciais, *Atmos. Meas. Tech.*, 2024, **17**, 4257–4290, DOI: **10.5194/amt-17-4257-2024**.
44 A. M. Collier-Oxandale, J. Thorson, H. Halliday, J. Milford and M. Hannigan, *Atmos. Meas. Tech.*, 2019, **12**, 1441–1460, DOI: **10.5194/amt-12-1441-2019**.
45 S. N. Riddick, D. L. Mauzerall, M. Celia, G. Allen, J. Pitt, M. Kang and J. C. Riddick, *Atmos. Environ.*, 2020, **230**, 117440, DOI: **10.1016/j.atmosenv.2020.117440**.
46 J. J. Y. Lin, C. Buehler, A. Datta, D. R. Gentner, K. Koehler and M. L. Zamora, *Environ. Sci.: Atmos.*, 2023, **3**, 683–694, DOI: **10.1039/d2ea00100d**.
47 W. Eugster, J. Laundre, J. Eugster and G. W. Kling, *Atmos. Meas. Tech.*, 2020, **13**, 2681–2695, DOI: **10.5194/amt-13-2681-2020**.
48 R. Rivera Martinez, D. Santaren, O. Laurent, F. Cropley, C. Mallet, M. Ramonet, C. Caldow, L. Rivier, G. Broquet, C. Bouchet, C. Juery and P. Ciais, *Atmosphere*, 2021, **12**, 107, DOI: **10.3390/atmos12010107**.
49 R. A. Rivera Martinez, D. Santaren, O. Laurent, G. Broquet, F. Cropley, C. Mallet, M. Ramonet, A. Shah, L. Rivier, C. Bouchet, C. Juery, O. Duclaux and P. Ciais, *Atmos. Meas. Tech.*, 2023, **16**, 2209–2235, DOI: **10.5194/amt-16-2209-2023**.
50 G. Domènech-Gil, N. T. Duc, J. J. Wikner, J. Eriksson, S. N. Påledal, D. Puglisi and D. Bastviken, *Environ. Sci. Technol.*, 2024, **58**, 352–361, DOI: **10.1021/acs.est.3c06945**.
51 A. Shah, O. Laurent, L. Lienhardt, G. Broquet, R. Rivera Martinez, E. Allegrini and P. Ciais, *Atmos. Meas. Tech.*, 2023, **16**, 3391–3419, DOI: **10.5194/amt-16-3391-2023**.
52 C. J. Jørgensen, J. Mønster, K. Fuglsang and J. R. Christiansen, *Atmos. Meas. Tech.*, 2020, **13**, 3319–3328, DOI: **10.5194/amt-13-3319-2020**.
53 A. Shah, O. Laurent, G. Broquet, C. Philippon, E. Allegrini, P. Kumar and P. Ciais, *Environ. Sci.: Atmos.*, 2024, **4**, 362–386, DOI: **10.1039/d3ea00138e**.
54 N. Bărsan, R. Ionescu and A. Vancu, *Sens. Actuators, B*, 1994, **19**, 466–469, DOI: **10.1016/0925-4005(93)01041-2**.
55 A. Shah, O. Laurent, G. Broquet, P. Kumar and P. Ciais, *ACS Omega*, 2024, **9**, 48323–48335, DOI: **10.1021/acsomega.4c06397**.
56 Figaro Engineering Inc.: Long2611CE Layout (1117).pdf, **https://www.figarosensor.com/product/docs/Long2611CELayout(1117).pdf**, accessed February 2025.
57 Picarro, Inc., G2401 Analyzer Datasheet | Picarro, **https://www.picarro.com/environmental/g2401_analyzer_datasheet**, accessed: April 2025.
58 A. Shah, O. Laurent, P. Kumar, G. Broquet, L. Loigerot, T. Depelchin, M. Lozano, C. Yver Kwok, C. Philippon, C. Romand, E. Allegrini, M. Trombetti and P. Ciais, *Atmos. Meas. Tech.*, 2025, **18**, 3425–3451, DOI: **10.5194/amt-18-3425-2025**.
59 A. Shah and P. Ciais, Data for "Characterising changes in methane response of a semiconductor-based metal oxide sensor over time", **https://zenodo.org/records/16573995**, accessed August 2025.